ACTIVE CONTROL OF SUBSONIC CAVITY FLOW USING PLASMA ACTUATORS

A Thesis

Presented in Partial Fulfillment of the Requirements for

Graduation with Distinction in the

Department of Mechanical Engineering at The Ohio State University

By

Nathan George Kamps

****

The Ohio State University

May 2007

Examination Committee:

Dr. Mo Samimy, Advisor

Dr. Igor Adamovich

Approved by

_____

Advisor
Department of Mechanical Engineering

ABSTRACT

Due to the prevalence of stealth technology on increasing numbers of new aircraft, weapons and electronics that had previously been stored under the aircraft wings are now being stored in weapons bays inside the fuselage. When these bays are opened however, a damaging flow situation can arise to create high amplitude pressure fluctuations capable of damaging structures and systems of the aircraft and the weapons stored in the bay. Thus a major area of research at the Gas Dynamics and Turbulence Laboratory (GDTL) has been focused on the suppression of these pressure fluctuations. Previous results using active flow control and a compression driver showed good flow authority up to Mach 0.40, when actuator effectiveness was lost. Other research at the GDTL has focused on the use of localized arc filament plasma actuators (LAFPA's) to control flow instabilities in a high Mach number free jet. The focus of this research was to incorporate the plasma actuators in a cavity flow facility and investigate their effectiveness at suppressing the tone generated by flows of higher Mach numbers. The results presented in this paper detail the results of testing several different actuator configurations on Mach 0.69 flow over a shallow cavity.

ACKNOWLEDGMENTS

I would like to thank Dr. Mo Samimy for all of his assistance throughout this project as well as providing me with the opportunity to do undergraduate research. I would also like to thank all of my colleagues at the Gas Dynamics and Turbulence Laboratory who have helped me with their technical expertise and their time for discussions and assistance. Most notable among these are Dr. Jin-Hwa Kim, Mike Snyder, Edgar Caraballo, and Jesse Little. I would also extend special thanks to Jeff Kastner and Doug Mitchell, without whom this project would not have been possible. Finally, I would like to thank my parents, siblings, and Amanda for their continual and unwavering support in all areas of my life.

VITA

May 19, 1984 …… Born – Cincinnati, Ohio

1998 - 2002 ……...…... St. Xavier High School – Cincinnati, Ohio

2002 – 2007 …….. Mechanical Engineering, The Ohio State University

FIELDS OF STUDY

Major Field: Mechanical Engineering

Minor Field: General Business

TABLE OF CONTENTS

LIST OF TABLES

Table **Page**

LIST OF FIGURES

Figure **Page**

CHAPTER 1

INTRODUCTION

Throughout a typical day, the average person comes into contact with many devices that utilize active control to maintain a desired output. Active control is characterized by the addition of energy into the system through some type of actuator. The thermostat in a house or oven, the cruise control on a car, and the autopilot on an aircraft are only a few of the devices that use this type of control. The prevalence of active control in everyday devices occurs because it has the ability to control many different types of outputs including current, voltage, temperature, velocity, altitude, and power. One field where active control is less robust however, is the area of flow control. Many methods have been used on aircraft and spacecraft to control flow but these almost universally involve moving an object such as the rudder, ailerons, or exhaust nozzle to achieve results. While energy is required to move these objects, no energy is added to the system so these cannot be classified as active control.

Currently a multidisciplinary team at the Collaborative Center for Control Science (CCCS), located at The Ohio State University, is investigating active flow control methods to reduce resonances created by flow over a shallow cavity. This research is being conducted with the Air Force Research Laboratory (AFRL) and the NASA Glenn

Research Center and is being conducted at the Gas Dynamics and Turbulence Laboratory (GDTL) located at OSU's Don Scott Airport.

Cavities are a feature common to most modern aircraft as they are often used for storage of retractable landing gear in large commercial airliners. Cavities have become even more common on military aircraft platforms in the last 20 years with the advent of stealth technology. Prior to this technology many aircraft carried weapons on external attachment points located under the wings or fuselage. This had the advantage of having many attachment points and allowing the weapons to be loaded and released easily. Incorporating stealth technology has the advantage of dramatically reducing the aircraft's radar cross section (RCS) but forces some design changes in other parts of the aircraft. Among these is the requirement for all weapons to be stored internally as the radar signature of external stores would greatly increase the aircraft's RCS. However, flow over the cavity presents a challenging problem as strong pressure fluctuations can be generated from the shear layer that forms as the flow of air separates from the cavity leading edge. This occurs when dynamics of the flow within the cavity couple with acoustic waves generated when the large-scale flow structures located within the shear layer interact with the cavity trailing edge. These acoustic waves travel upstream where they interact with the shear layer as it forms near the leading edge (Debiasi and Samimy, 2004). The result is a self-sustaining, resonant system that can produce pressure fluctuations strong enough to damage structures and systems of both the aircraft and the stores. These pressure fluctuations have also been shown to increase drag on the cavity by as much as 250% (McGregor and White, 1970) and can cause erratic motion of released stores (Bjorge et al., 2005). These can be severe enough to cause a phenomenon

known as “recontact” where the weapon is thrown upwards into the aircraft it was just released from.

Previous research into active control of cavity flows conducted at the GDTL had focused on the use of a synthetic-jet type actuator created through the use of a compression driver. This actuator was able to suppress the dominant resonant tones in the cavity by as much as 20 dB without producing other resonant tones. Baseline data on the optimum forcing frequencies for tone reduction were used to create a closed loop controller able to maintain optimum forcing in a changing flow situation. The actuator was found to be effective for Mach numbers up to 0.40 (Debiasi and Samimy, 2004). Given the decline in actuator authority at Mach numbers greater than 0.40, it was thought that a more powerful actuator was required to achieve similar peak reductions for higher Mach number flows. As the compression driver was limited by both frequency bandwidth and output power, an alternative actuator was desired for a higher Mach number facility (Mitchell, 2006).

Based on the conclusions of other research also being conducted at the GDTL, localized arc filament plasma actuators (LAFPA’s) were selected as the actuator for higher Mach number experiments for cavity flow control. These actuators were found to be very successful for active control of a high speed jet (Samimy et al., 2007). They also have the advantage of large bandwidth, high amplitude actuation while also having small size (Mitchell, 2006). LAFPA’s are essentially two electrodes placed a small distance apart with the air gap in between acting as a resistor. When a large voltage is applied between the electrodes, an electrical arc occurs between them. Rapid heating of the air is near adiabatic and creates a rapid pressure increase that can be used to control flow

instabilities in the jet. It was hypothesized that this phenomenon could be also applied to cavity instabilities that produce resonant tones. Experiments performed with 3 plasma actuators across a 1.5 inch cavity showed that the actuators had influence over the flow, but were not powerful enough to disrupt the resonant tones (Mitchell, 2006). The goal of further research then became to place more actuators along the cavity leading edge with the hypothesis that more actuators would result in a stronger influence over the flow.

This thesis addresses the research conducted on a high speed cavity model using increased numbers of plasma actuators. The facility was first run without plasma to find both resonant and non-resonant baseline flow conditions. The setup was then run with actuation and the effects of the actuators on the flow were studied to determine their authority.

CHAPTER 2

BACKGROUND

2.1. – Introduction

Since research of cavity flows requires an understanding of many different engineering disciplines, the following review is included to familiarize the reader with some of the concepts most critical to this effort. These topics include cavity flow physics, control theory, and plasma actuation.

2.2. – Cavity Flow Physics

The study of cavity flow physics began in the 1950's and has continued to the present day (Cattafesta et al., 2003). The first applications were flow over the bays that housed retractable landing gear. While this is perhaps the most common application today, cavity flow has many other applications from flow over weapons bays and optical ports on aircraft to flow over sunroofs and windows in modern automobiles. Strong pressure fluctuations that arise from the flow can create dynamic loads in excess of 160 dB (using a reference pressure of 20 μPa). These pressure fluctuations can be damaging to structures and systems of both the cavity contents and the airframe itself (Bjorge et al., 2005). Finally this can also create problems with the release and accurate delivery of weapons stores contained within the cavity. This problem is exacerbated by the trend in

recent years to “smart-bombs” which are smaller and lighter than ever before (Cattafesta et al., 2003). These weapons contain sensitive electronics that can be damaged by strong pressure fluctuations. In addition, the flight path of a lighter weapon is more easily disturbed when it passes through the shear layer than that of a heavier weapon.

Since cavities have a uniform cross section, they are generally treated as 2-D by considering only the longitudinal (flow) direction and the transverse (cavity depth) direction as shown in Figure 1. Furthermore, cavities are typically sub-divided into two groups based on the aspect ratio, L/D, where L is the cavity’s length in the direction of flow and D is the cavity depth. Cavities with aspect ratios less than 1 are considered deep while those with greater than 1 are considered shallow. Since deep cavities were not considered in this research, this discussion focuses only on shallow cavities.

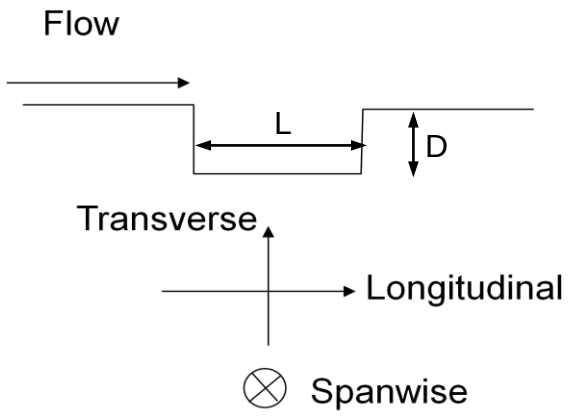

Figure 1: Cavity Orientation

The pressure fluctuations generated by cavity flows arise from the shear layer that develops when the flow encounters the discontinuity formed by the leading edge of the cavity. Since the flow cannot turn sharply to enter the cavity, it detaches over the cavity span and reattaches at the trailing edge. The shear layer contains rolling turbulent

structures that are generated by the difference between the low velocity fluid in the cavity and the high velocity flow above the cavity. This phenomenon is referred to as the Kelvin-Helmholtz instability. The shear layer travels downstream until it reaches the cavity trailing edge, where it reattaches. The impingement of the shear layer on the trailing edge of the cavity produces acoustic waves which then travel upstream and to the receptivity region of the shear layer as it forms near the leading edge of the cavity as shown in Figure 2. This receptivity region is the area most susceptible to external inputs (Pope, 2000). The coupling of the shear layer pressure fluctuations and the cavity acoustic thus forms a feedback system that is reinforcing and self-sustaining. This feedback loop produces the strong pressure fluctuations that are generally characterized by a single dominant tone however multiple modes and mode switching can also occur. A block diagram of the acoustic feedback loop is shown in Figure 3 below.

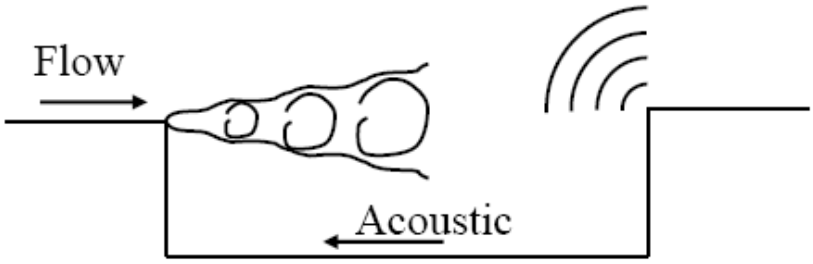

Figure 2: Shallow Cavity Feedback Generation Mechanism (Little, 2004)

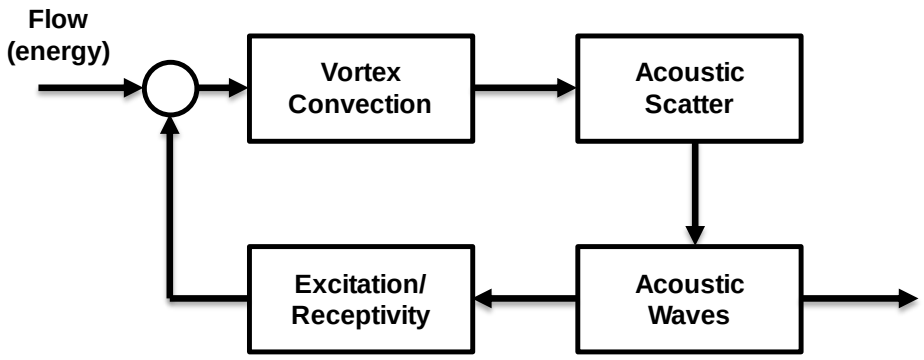

Figure 3: Block Diagram of Shallow Cavity Acoustic Coupling (Little, 2004)

In the 1960's J.E. Rossiter developed a semi-empirical formula that can be used to predict the dominant frequencies of pressure fluctuations generated by the turbulent structures in the shear layer (Rossiter, 1964.) This equation is shown in non-dimensional form in terms of Strouhal number in Equation 1 below:

$$St_n = \frac{f_n L}{U_\infty} = \frac{n - \varepsilon}{M_\infty \left\{1 + \left[\frac{\gamma - 1}{2}\right] M_\infty^2\right\}^{-1/2} + \frac{1}{\beta}} \quad (1)$$

where f is frequency, L is the cavity length, U_∞ and M_∞ are the freestream velocity and Mach numbers respectively, n is the integer number of large-scale flow structures spanning the cavity, ε is the phase lag, γ is the ratio of specific heats, and $\beta = U_c / U_\infty$ is the ratio of the convective speed of the large scale structures to the freestream velocity. For this research the cavity dimensions were L = 1.00" (25.4 mm) and D = 0.25" (6.35 mm). Additionally prior research has shown that ε = 0.25 and β = 0.66 (Rossiter, 1964). Some critics have pointed out that Rossiter's equation does not include shear layer thickness and cavity depth (Williams et al., 2002). It also does not predict the amplitudes of the tones that are generated, but despite these shortcomings, Rossiter's equation has shown success in predicting resonant frequencies. Because of this, these frequencies are

referred to as Rossiter modes and the Rossiter equation remains the governing equation for cavity flow physics.

The second important consideration is the prediction of the acoustic modes that couple with these Rossiter modes to produce cavity resonance. Since the speed of a one dimensional pressure wave is constant, namely the speed of sound, and the cavity geometry is known, these modes can be predicted by half wave length theory (Mitchell, 2006). This simply involves a calculation based on the distance between the nodes for the mode in question (Halliday et al. 2002). Thus the one-dimensional acoustic modes may be predicted as shown in terms of Strouhal number as shown in Equation 2 below:

$$St_n = \frac{f_n L}{U_\infty} = \left(\frac{L}{h}\right)\frac{n}{2M_\infty} \qquad (2)$$

where f is frequency, L is the cavity length in the direction of flow, h is the length between nodes, U_∞ and M_∞ are the freestream velocity and Mach numbers respectively, and n is the integer mode number. This formula can be used to predict all of the modes in the longitudinal, transverse, and lateral directions. In the 1970's it was found that a single dominant mode tends to occur when Rossiter modes coincide with longitudinal acoustic modes that are determined by the cavity length (Rockwell and Naudascher, 1978). This does not preclude resonance from occurring at the intersection of Rossiter modes and the other acoustic modes however. Past research at the GDTL has investigated control of tones generated with the transverse acoustic mode (Debiasi and Samimy, 2004); as will be subsequently shown, the tone obtained with this research also occurs due to the interaction of the Rossiter mode with the 1st transverse mode. It has also been suggested that multi-mode resonance arises for cases when Rossiter and acoustic modes do not intersect (Williams et al., 2000). While the intersection of

Rossiter modes and longitudinal modes provides a good prediction for where resonance may occur, it should be noted that resonance can occur at other modal intersections. Furthermore, while this is currently the best prediction method available, experimentation is still required to verify these predictions. Figure 4 below shows the predicted Rossiter and acoustic modes for the cavity tested.

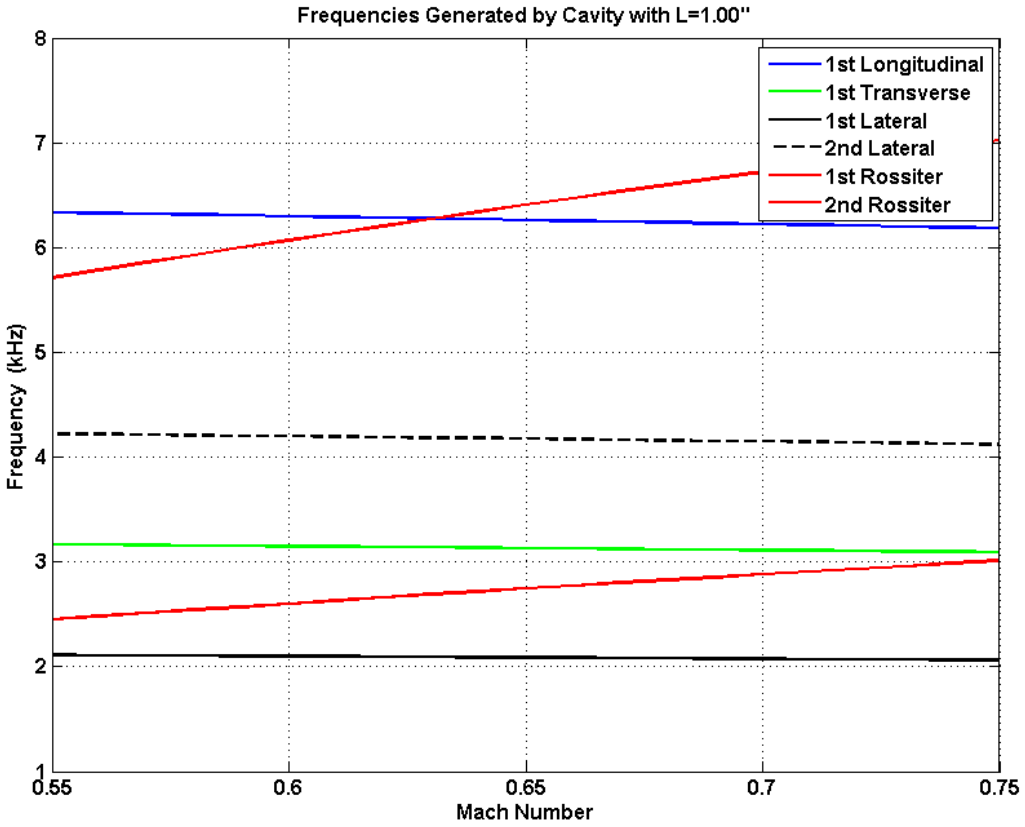

Figure 4: Predicted Rossiter and Acoustic Modes

2.3. – Control Techniques

Once the cavity resonant modes are predicted, a natural next step is to address how these modes may be controlled. Control methods are divided into two major

categories: passive and active. As discussed previously, active control involves adding energy to the flow through the use of some type of actuator while passive control involves no energy addition. Thus passive techniques usually involve geometric modifications through the use of fences, ramps, screens, or cylinders placed near the cavity's leading edge. Generally the goal of these modifications is to thicken the shear layer or move the location of reattachment. This avoids or reduces the strength of impingement of the shear layer on the cavity trailing edge (Williams et al., 2002) thus reducing the strength of the acoustic feedback mechanism. Passive controls have the advantage of being simple, inexpensive and reliable. Unfortunately they cannot adapt to a changing flow situation and may be ineffective or even increase resonance at off-design conditions.

In contrast, active controls are more complicated and expensive but have the capability to adapt to a variety of flow conditions. Active control requires that energy be added to the flow through some type of actuator whose output can be varied. This ability to vary the output of the actuator allows active control methods to be more versatile and to adapt to a changing environment. The method used to control this output is the basis for a further division of active control into two categories: open-loop and closed-loop. In open-loop control the output of the actuator is typically adjusted by an operator or uses a look-up table to obtain desired results. On the other hand, closed-loop control involves using data from one or more sensors in the system to create a feedback loop. A good example of the differences between open and closed-loop control is manual control of automobile speed by the driver versus the use of cruise control. A chief advantage of closed-loop control is that it removes the need for adjustment by an outside operator and

frequently allows for a faster time response as a controller can operate much faster than a human. Finally, closed loop control requires approximately one order of magnitude less power than open-loop control (Cattafesta et al., 1997).

Open-loop control was selected for use in this research project since it was an early implementation of a new type of actuator for cavity flow control. Thus the response of the cavity to this actuation was not well known. If open-loop control was shown to be effective in suppressing resonant tones, the results of this experiment could then be used to design a closed-loop controller. It is important to note that the development of a closed-loop system, capable of reducing cavity resonance in a changing flight environment and being implemented by an aircraft on-board computer, is a major long range goal of the broader research team at the GDTL.

2.4. – Plasma Actuation

An actuator can be effective in controlling cavity resonance only if it is capable of significantly influencing the shear layer. This is accomplished by providing an input of sufficient amplitude at frequencies in the instability free range. This causes the prevalence of smaller structures in the flow to increase and accelerates the rate of energy transfer from the larger scale structures to the smaller structures resulting in viscous dispersion. This results from conservation of energy and the transfer disrupts the large scale structures which cause strong resonant tones (Mitchell, 2006). Unfortunately, two other important phenomena can occur to decrease the effectiveness of actuation. The first, referred to as peaking, is when actuation causes the resonant tone to be reduced but the actuation induces another resonant tone of comparable strength at a different

frequency. Peak splitting is a similar phenomenon which occurs when the resonant tone is reduced and multiple strong resonances at other frequencies are induced by the actuation (Debiasi and Samimy, 2004).

Several types of actuators have been found to be effective for active flow control including piezoelectric flaps (Cattafesta et al., 2001), synthetic jets (Little et al., 2006), and plasma actuators (Samimy et al., 2004). Selection of a proper actuator is a crucial element of an effective control strategy as the actuator often limits the effectiveness of the entire control system. This is evidenced by the loss of effectiveness of a synthetic jet actuator at Mach numbers greater than 0.40 despite significant attenuation of cavity tones at lower Mach numbers (Debiasi and Samimy, 2004). This led to the conclusion that the synthetic jet used was not powerful enough to attenuate resonances at higher Mach numbers, regardless of the effectiveness of the controller used. This required that a more effective actuator be found for high Mach number flow control. At the same time, another research effort at the GDTL suggested that localized arc filament plasma actuators (LAFPA's) could be effective in controlling supersonic flows (Samimy et al., 2006). Given this, LAFPA's were selected for use in this project with the hope that they would exhibit similar robustness in the control of cavity flows.

LAFPA's work through a rapid, nearly adiabatic, local heating of the flow that causes a rapid increase in pressure. The plasma can be turned on and off at high frequencies to vary how pressure spikes from the plasma affect the instabilities in the flow. Prior to the development of LAFPA's, most plasma actuation methods used DC, AC, RF, microwave discharges or laser breakdown (Utkin et al., 2007). The primary

disadvantage of these methods is that they are only applicable for low Mach numbers (Mitchell, 2006).

LAFPA's have several advantages over other type of plasma actuation as they are very small, can operate in both subsonic and supersonic flows, have large bandwidth of operation, and produce high amplitude pressure fluctuations. Typically, LAFPA's consist of two electrodes placed with their ends approximately 3 mm apart. One electrode acts as the cathode or "hot" wire and the other is the anode or "ground" wire. To turn the plasma on, a large voltage (about 10,000 V) is applied to the cathode to produce an electrical arc between the electrodes. This arc ionizes the air in the flow, creating plasma at about 2000 °C. This rapidly heats surrounding air and creates the desired pressure increase. In order to place more actuators along a given cavity length, each plasma actuator for this research effort consists of two cathodes which share a common anode placed in between. This allowed 5 actuators to be placed across the 3.0 inch cavity span requiring 10 cathodes and 5 anodes. This setup provided 53% coverage across the cavity span.

CHAPTER 3

EXPERIMENTAL METHOD

3.1. – Experimental Facility

All of the experiments involved in this research were performed at the Gas Dynamics and Turbulence Laboratory (GDTL) located at The Ohio State University's Don Scott Airport. Two four-stage compressors provide air for the blow down type facility which is capable of continuous operation. Two cylindrical tanks with a capacity of 36 m^3 store air which has been dried, filtered, and compressed to a maximum pressure of 16 MPa. The air enters the facility test section via a stagnation chamber and a converging nozzle. After exiting the facility, the air exhausts to the atmosphere. A solenoid valve is used to control the stagnation pressure in the chamber to within ± 0.10 psig.

The test section of the high speed facility was manufactured in the summer of 2006 and modified for this research study. Figure 5 shows the exterior of the high speed test section installed at the GDTL. Two primary parts compromise the cavity: the Kulite housing and the plasma actuator extension. These can be seen in the solid model of the test section shown in Figure 6. Each of these parts will be discussed separately.

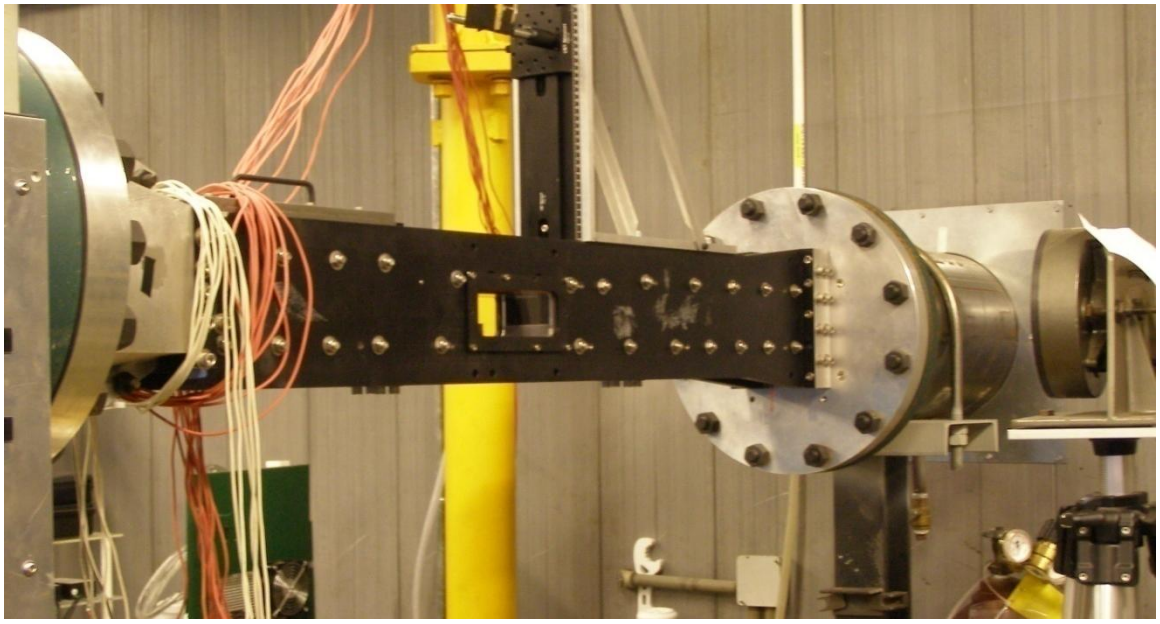

Figure 5: Experimental Facility

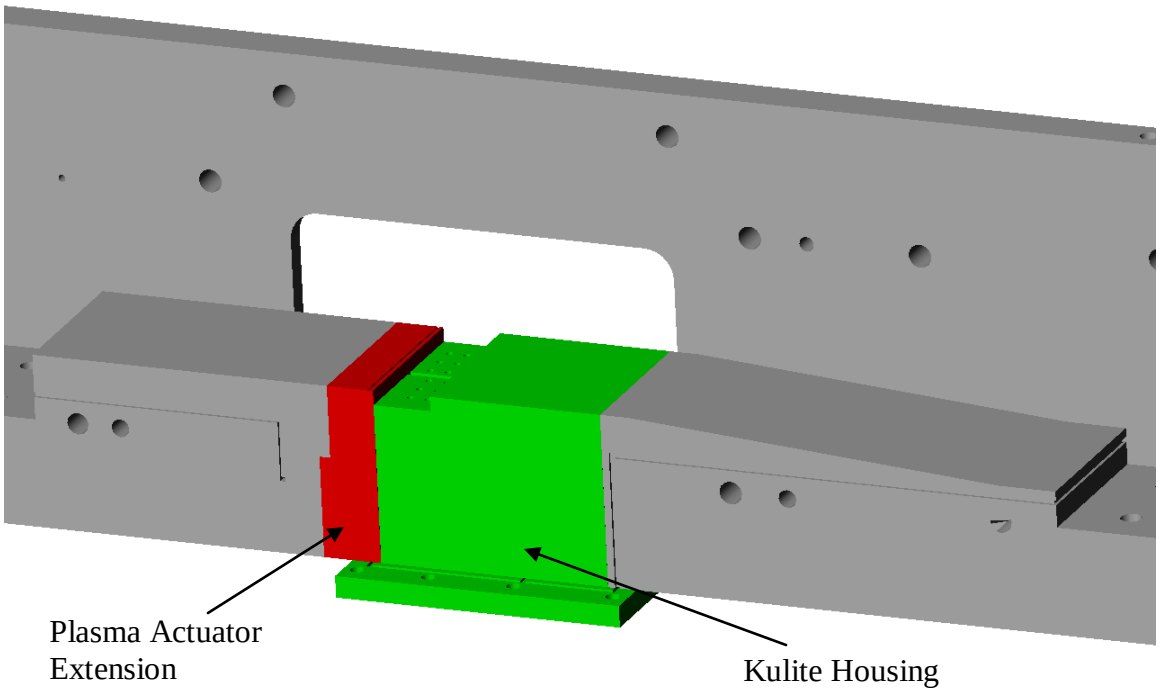

Figure 6: Solid Model of Cavity Test Section

3.2. – Kulite Housing

As shown in Figure 6, the Kulite housing compromises the cavity floor and trailing edge sections. The part is hollow in order to allow the Kulite pressure transducers to be easily accessed. Up to 15 Kulites can be inserted in the cavity floor simultaneously and the Kulites are labeled as shown in Figure 7 which also shows a picture of the fabricated part. More details of the setup for data acquisition can be found in section 3.4.

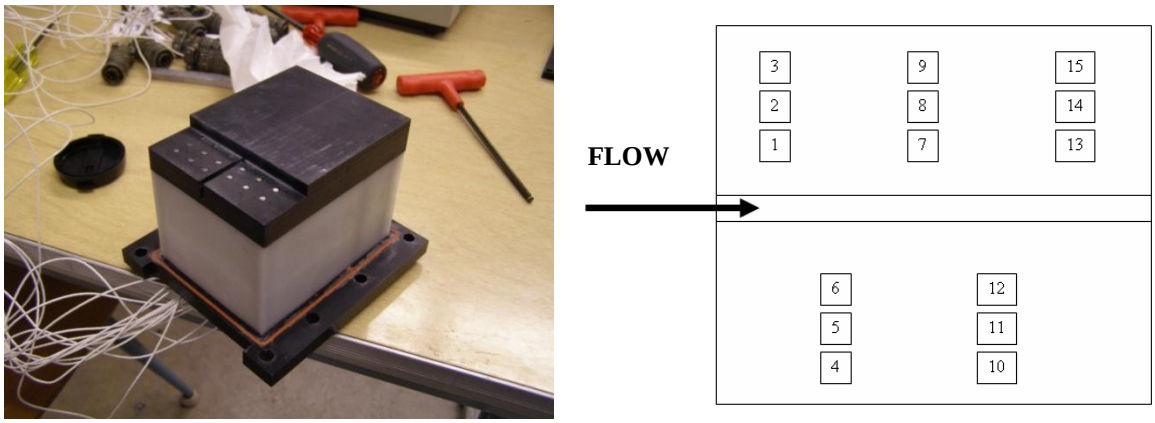

Figure 7: Fabricated Kulite Housing and Kulite Numbering Scheme

Other features of note on the Kulite housing include the groove between the two groups of Kulite ports and the lip at the bottom of the housing. The groove disperses light of a laser sheet used when conducting PIV measurements. The lip at the bottom of the housing overlaps with the bottom of the plasma actuator extension to hold it in place. This serves as a backup to protect the delicate plasma extension from falling out if the bolts securing it should fail.

3.3. – Plasma Actuator Extension

As can be seen in Figure 6 on page 16, the plasma actuator extension also forms the cavity leading edge and forward wall. The extension is made of boron nitride, a machinable ceramic capable of withstanding the high temperatures created by the plasma without degradation. Despite these advantageous features, boron nitride is both expensive and very brittle and so must be handled with care. To reduce the chances that the extension would be damaged during handling, it is mated to a plastic adapter piece using 5 nylon bolts. It is this adapter piece that is then handled to prevent damage to the extension. The 3 bolts that secure the extension in the facility are also located in the plastic adapter. These can be seen in Figure 8 which shows the mated plasma extension and adapter. A part similar to this assembly was also created entirely from plastic for experiments that did not require plasma actuation. This part replaced the adapter – extension assembly further protecting the boron nitride from unnecessary handling.

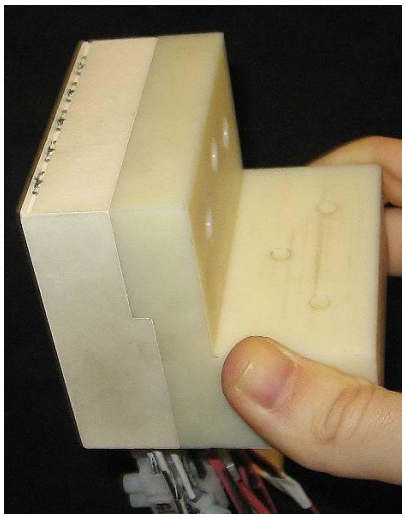

Figure 8: Plasma Actuator Extension Mated to Plastic Adapter

The extension contains 15 holes to hold the 1.00 mm tungsten electrodes for the plasma actuators. As discussed in section 2.4, each plasma actuator consists of two cathodes which share a common anode. To prevent unintended arcs between two cathodes in adjacent actuators, the spacing between the actuators was slightly larger (5.00 mm) than the spacing between the cathodes and anodes (4.00 mm). Similarly, extra spacing was added between the cathodes and the facility wall to prevent unintended arcs. This can be seen in Figure 9 which shows a solid model of the plasma actuator extension with the cathodes and anodes on one actuator labeled. This pattern repeats four more times across the entire length of the cavity leading edge. Figure 10 shows a close-up of the installed electrodes on the fabricated part. Also visible is the groove that the actuators are located in. This groove allows the plasma to fully develop without being blown downstream by the high velocity air. Appendix A contains the engineering drawings for the plasma actuator extension.

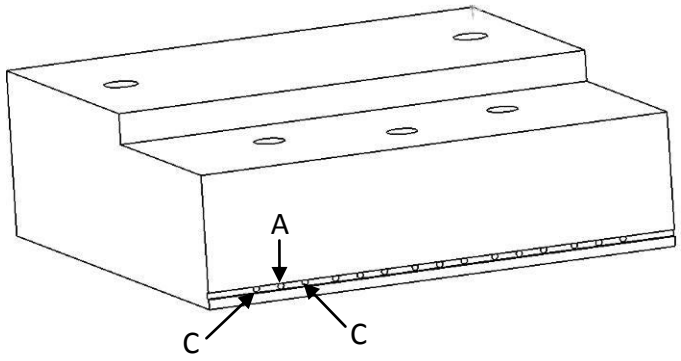

Figure 9: Solid Model Showing Electrode Positions (C - Cathode A - Anode)

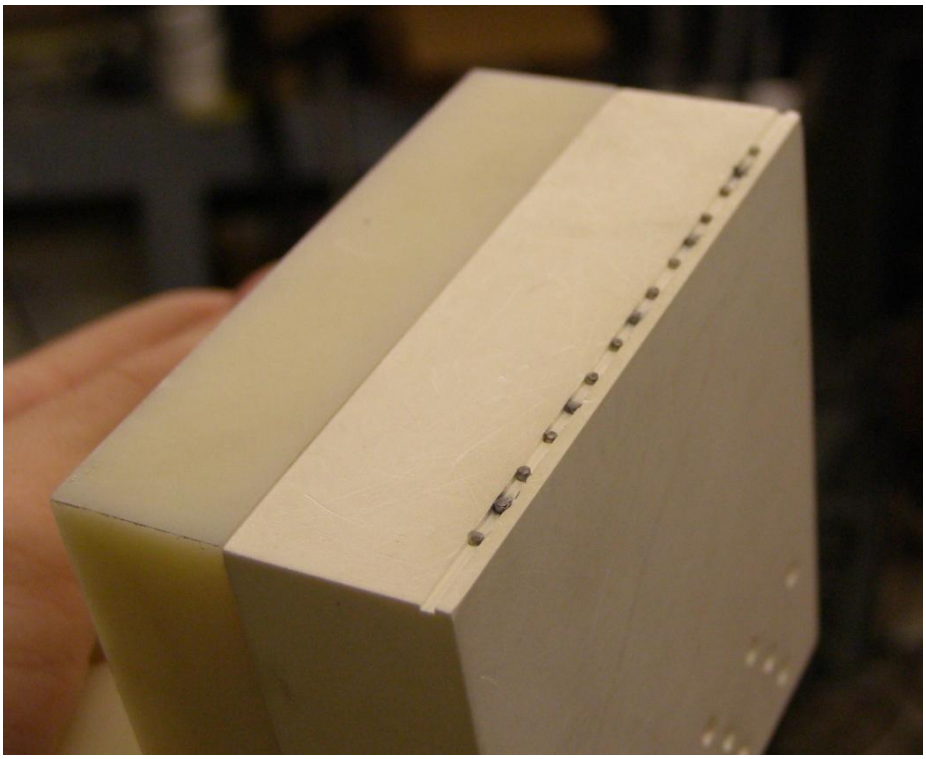

Figure 10: Close Up of Plasma Actuator Extension Showing Electrodes

Despite the proper separation of electrodes and the high resistance of the boron nitride, it is still possible for electrical arcs to occur in undesirable locations so precautions against this are incorporated in the design. All of the holes for the electrodes are tilted aft to make manufacture of the part easier. The 5 anode holes have a slightly larger angle than the 10 cathode holes, and therefore are located slightly farther aft than the cathode holes. This maximizes the separation of the cathodes and anodes as they emerge from the bottom of the extension, making arcing there significantly less likely.

It is also possible for an arc to be generated between the electrodes within the extension which would destroy an interior portion of the boron nitride. This type of anomaly would be difficult to detect afterward and the destruction of the material would make future arcs in that location far more likely and could cause difficulties in obtaining

proper arcing near the cavity leading edge. To guard against this the electrodes are painted and wrapped in paper to increase the resistance between the anode and cathode. The paint used is automotive touch-up paint typically applied in two coats. The paint is removed from the ends of the electrodes using sandpaper to encourage arcing at the proper location. Additionally, small strips of paper are wrapped around the electrodes and slid into the bottom of the extension to further increase the resistance to arcing. Finally both the paint and paper provide a method of detecting internal arcs after they have occurred due to the burn-through of paper and removal of paint that is visible when these arcs occur. Figure 11 shows the installed cavity as viewed through the facility windows. Both the plasma actuator extension and Kulite housing can be seen. Additionally, the paper wrapped electrodes and lead wires may be seen emerging from the extension near the bottom of the frame.

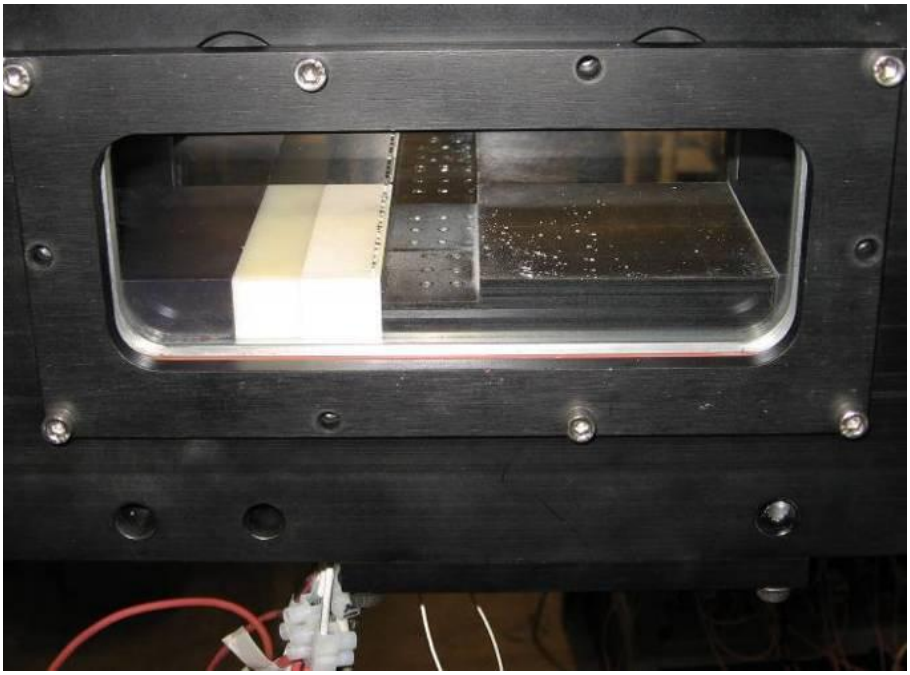

Figure 11: Installed Cavity Viewed through Facility Windows

3.4. – Data Acquisition (DAQ)

As discussed in section 3.2, up to 15 Kulite pressure transducers can be embedded in the cavity floor simultaneously for obtaining time resolved pressure measurements. Due to concerns that unintended arcs could occur between the actuators and the Kulites, only transducers 7 and 13 (as numbered in Figure 7) were used to gather data. Ectron Model 563HL amplifiers are used to power the Kulites and also provide a gain of 10 to the signal. The signal is then high pass filtered with Kemo VBF21M configuration model 21M/10/37 filters. A National Instruments PXI-6143 data acquisition system is then used to acquire the data which is recorded using LabVIEW.

This configuration is capable of sampling up to 24 channels at 16 bit resolution and a sampling frequency of 250 kHz. For all experiments conducted in this research, pressure measurements were taken in blocks of 819,200 continuous samples using 16 bit resolution and a 200 kHz sampling frequency. This allows a frequency resolution of approximately 24 Hz. Matlab is then used for data analysis including converting the voltage signal to pressure using the sensitivity for the Kulites of 4 mV/psia. The sound pressure level (SPL) can then be found using Equation 3 below:

$$L_P = 20 \cdot \log_{10}\left(\frac{P_{RMS}}{P_{REF}}\right) \tag{3}$$

where L_P is the sound pressure level, P_{RMS} is the root-mean-square pressure, and P_{REF} is the reference pressure of 20 μPa. The SPL can then be resolved to the frequency domain by taking a Fast-Fourier Transform (FFT). This can then be compared to the predicted frequencies as shown in Figure 4.

Due to strong electromagnetic interference (EMI) signals that arise from the high voltages used in plasma generation, an altered DAQ system was used to obtain accurate

measurements. For this setup an in-house conditioner was used to power the Kulites, and provide gain and low-pass filtering capability. The signal was acquired using the same National Instruments PXI-6143 system and was digitally high pass filtered in Matlab.

3.5. – Plasma Generation

An in-house plasma generation system shown in Figure 12 below is used to provide the required voltage signals to the LAFPA's. The system can operate up to 12 cathodes independently; the anodes are not connected to the system. Instead each anode is connected to ground via the building structure. For added safety, the anodes are connected to two ground sources in case one of the grounds is inadvertently disconnected. The cathodes are powered by two high-current, high-voltage DC Glassman High Voltage Inc. power supplies. Each channel is controlled by a fast response, high repetition rate, high-voltage, water-cooled MOSFET transistor switch with two 15 kΩ high power solid body ceramic resistors connected in series (Utkin et al., 2007). The transistors are controlled by a computer capable of independently controlling the phase and duty cycle of each transistor.

While the phase of each actuator could be varied, this research was limited to no phase shift between actuators meaning all 5 actuators were firing simultaneously. Similarly, while the duty cycle could be varied for a given forcing frequency, this research was limited to actuation signals of the form X kHz – X% duty cycle. For example, forcing signals tried include 3 kHz – 3% duty cycle and 10 kHz - 10% duty cycle. This maintains a constant time of 10 μs for each period of plasma generation. Since the period of plasma generation is constant however, as frequency increases, the

cooling time for the electrodes decreases. This caused electrode degradation at high forcing frequencies and, as will be discussed in subsequent sections, proved to be a limiting factor for which forcing frequencies could be successfully tested.

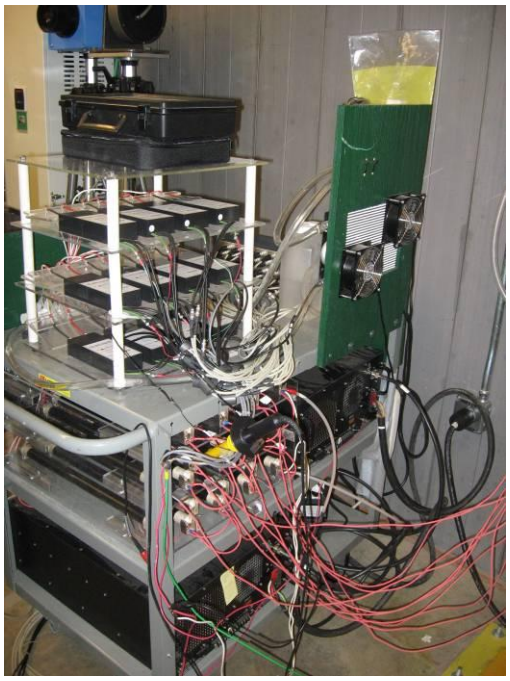

Figure 12: Plasma Generation System

Two different wiring schemes were also used for plasma generation. Schematics of both are included in Appendix B. The first utilized 1 transistor to run each actuator therefore each MOSFET controlled 2 cathodes. During testing it was noticed that this produced uneven arcing that was able to be detected visually through the facility windows. Typically one cathode-anode combination would produce plasma, while the other cathode-anode set on the same actuator would not. This was not acceptable so the wiring was changed so that each transistor controlled only one cathode with the control computer used to properly synchronize the signals to each transistor. This proved to be a

much more effective setup and all actuators showed proper arcing when viewed through the facility windows.

CHAPTER 4

EXPERIMENTAL RESULTS

4.1. – Cavity Characterization

Before experimentation could be conducted with the plasma actuators, it was first necessary to characterize the flow over the cavity as a function of Mach number. In addition to using this data to select baseline cases, the characterization allows comparisons to be made to the predictions shown in Figure 4. For this cavity, a Mach sweep was performed from 0.60 to 0.95. The Kulite data was used to determine how the freestream Mach number varied along the length of the cavity as shown in Figure 13. For Mach numbers between 0.60 and 0.72, a 2% or less change in Mach number was observed. At higher Mach numbers, a larger increase in freestream velocity can be seen. This is due to the growth of the shear layer as it travels downstream from the cavity leading edge. This effect reduces the available area for the freestream flow and forces an increase in velocity since the flow is subsonic. In order to have a flow with uniform velocity over the cavity length, it was decided to narrow the baseline case selection to Mach numbers less than 0.72.

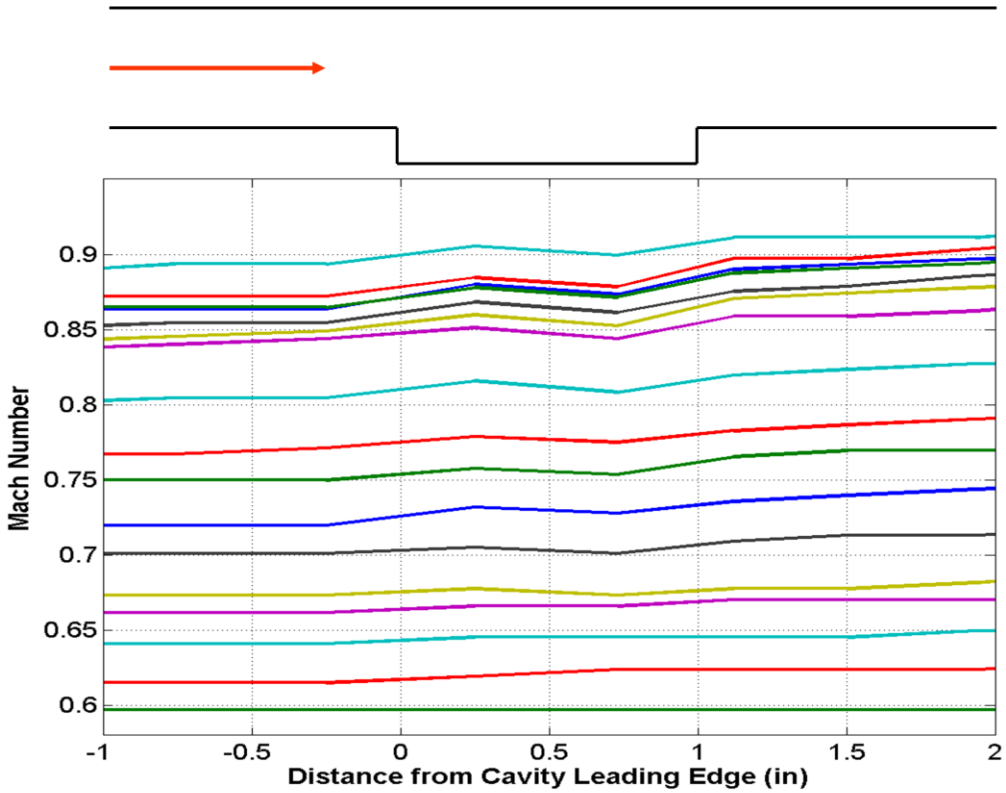

Figure 13: Freestream Mach Number Variation in Flow Direction

Following this the Kulite data was used to calculated sound pressure level (SPL) and plotted in the spectrogram in the right half of Figure 14 which shows the amplitude of pressure fluctuations as a function of Mach number and frequency. As indicated by the color scale at right, blue indicates smaller pressure fluctuations while yellow and red indicate larger pressure fluctuations and possible tone generation. When overlayed with the previously discussed predictions (repeated for convenience in the left half of Figure 14), good comparison is observed. As seen in this comparison, the cavity is generating a tone at Mach numbers greater than 0.62 via the intersection of the 1st Rossiter and 1st transverse acoustic modes at approximately 3 kHz with a harmonic appearing at approximately 6 kHz.

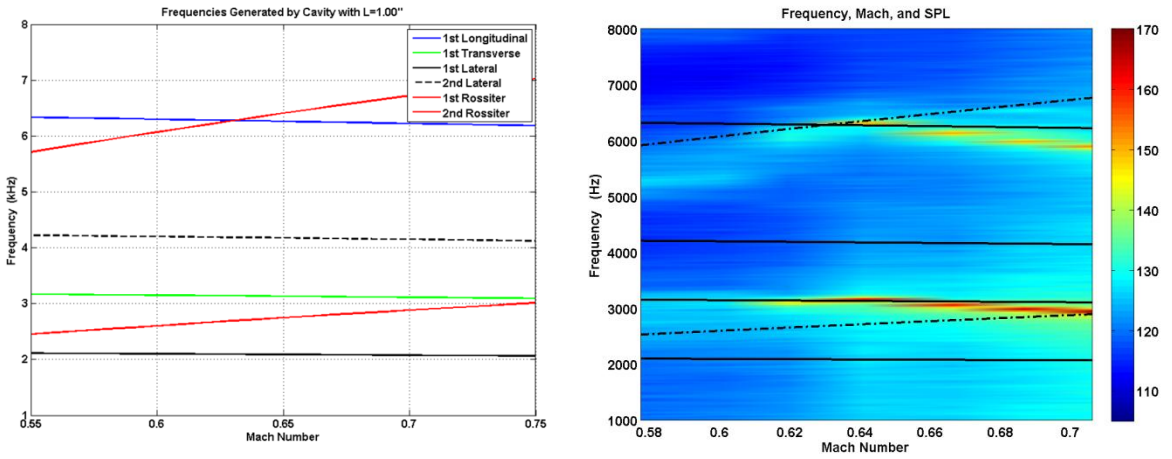

Figure 14: Comparison Between Predicted Resonances and Spectrogram

In addition to the Kulite measurements taken, Schlieren photographs were also taken, several of which are shown in Figure 15. Comparison between the Mach 0.60 and Mach 0.69 cases illustrates the changes that arise in the flow when resonant tones are generated. At Mach 0.60, the lack of resonance is illustrated in the disorganized nature of large-scale structures in the shear layer. This is contrasted with the Mach 0.69 case where the shear layer appears as nearly a half-sine wave. The Mach 0.72 case is of interest due to the spurious Mach waves. This is a similar effect to the Mach number variation over the cavity discussed above, but is due to the boundary layer growth at the tunnel entrance which reduces the flow area and produces localized sonic flow.

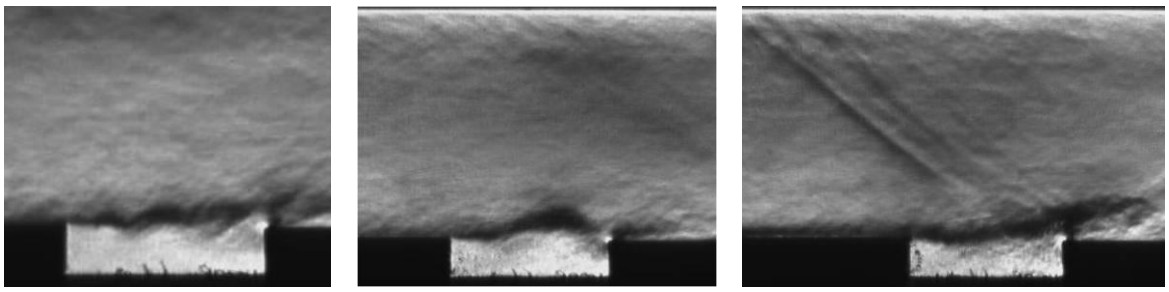

M = 0.60 **M = 0.69** **M = 0.72**

Figure 15: Instantaneous Schlieren Photographs for Selected Mach Numbers

In selecting baseline cases, it was also necessary to avoid cases where Mach waves were generated since these would affect the pressure fluctuations in the flow field. Thus the selection of baselines was limited to Mach numbers below 0.72. Since the characterization was performed with the plastic insert in place of the plasma actuator extension, the SPL's with the correct extension were checked to verify that this change had no effect on the spectrum. Figure 16 shows the spectra for both baselines obtained with the plasma actuator extension which were verified to be identical to those obtained with the plastic insert. The Mach 0.60 case exhibits no strong tones and has broadband noise between approximately 120 and 130 dB. The Mach 0.69 case exhibits a strong resonant tone of over 160 dB generated at 3 kHz with harmonics appearing at 6 kHz and 9 kHz. As a result, the Mach 0.69 flow was selected as the resonating case and the Mach 0.60 flow was selected as the non-resonating case. For the remainder of this paper, all spectra obtained with plasma actuation will be compared to these baselines. Since this research effort is concentrated on suppression of resonant tones the focus of the results is the effect of the actuators on the Mach 0.69 case.

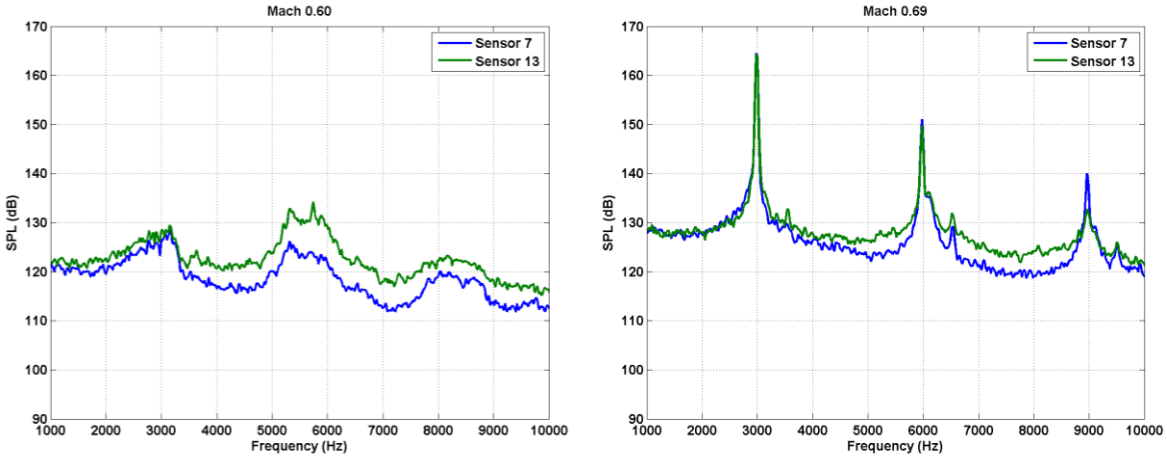

Figure 16: SPL Spectra for Non-resonating and Resonating Baselines

4.2. – Initial Testing: 1 mm Anode

For the initial plasma actuator extension design which utilized 1 mm tungsten electrodes, forcing frequencies from 1 to 10 kHz were tested at 1 kHz intervals. As discussed above, the frequencies were limited to those of the form X kHz – X% duty cycle in order to maintain a plasma pulse time of 10 μs. Figure 17 shows the SPL for the 8 kHz – 8% duty cycle case and the 8 kHz tone produced by the plasma actuation can be seen to be 150 dB. The spectrum only shows a 3 dB reduction in the tonal amplitude however, and similar results were obtained for all frequencies between 1 and 10 kHz. The reduction of the 3 kHz tone for each forcing case (as measured by both sensor 7 and 13) is shown in Figure 18.

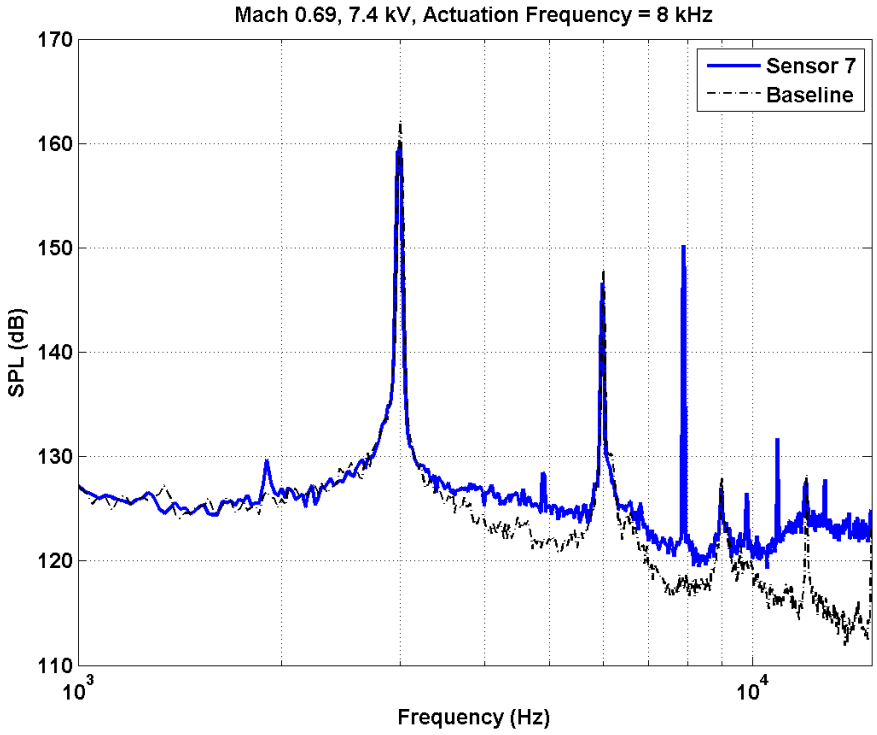

Figure 17: Mach 0.69 - 8kHz forcing - 1 mm anode

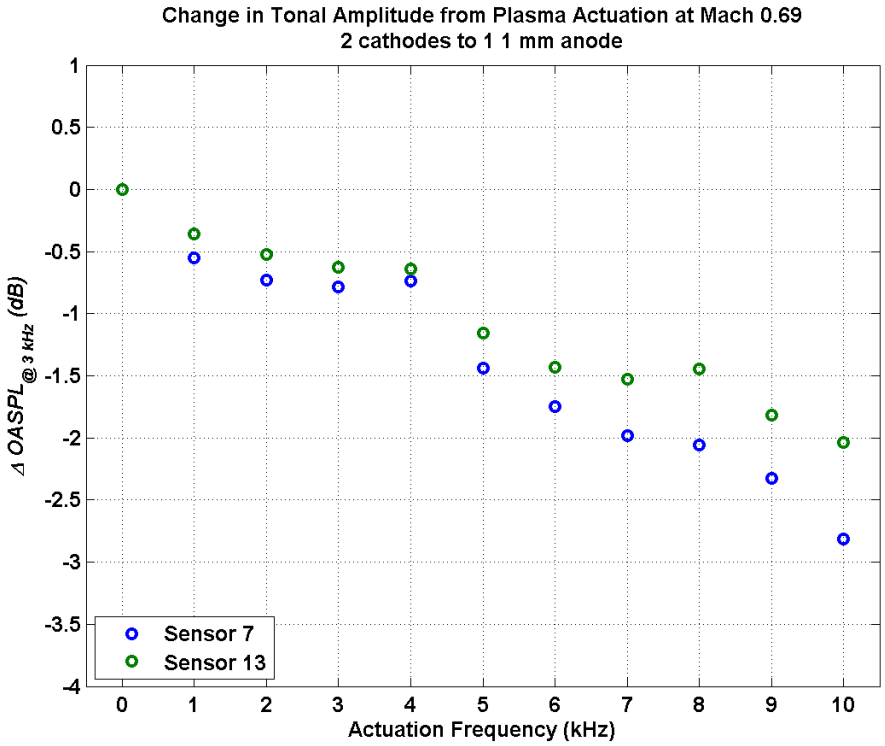

Figure 18: Change in Tonal Amplitude with 1 mm Anode

As seen in Figure 18, the reduction in tonal amplitude increases with increasing forcing frequency with a maximum reduction of about 3 dB at 10 kHz forcing. Despite having reduced the resonant tone in all cases, the amount of reduction was significantly less for all cases than the 20 dB reduction that has been demonstrated with different actuators (Debiasi and Samimy, 2004). With this in mind, it was decided to experiment with higher forcing frequencies up to 40 kHz. When this was tried however, the plasma actuators stopped arcing at frequencies above 12 kHz due to erosion of the electrode and the insulating paint. This effect is shown in Figure 19 where an eroded electrode (top) is contrasted with an unused electrode (bottom). Additionally, run times were limited to about 10 minutes before arcing ceased, regardless of forcing frequency. Following this it was necessary to remove, sand, and repaint the electrodes before they could be

reinstalled. At best this procedure took several hours. After repeated attempts consistently showed electrode erosion, it was theorized that the common ground electrode was too small to handle the current of arcs from both cathodes. This is exacerbated at higher forcing frequencies due to the constant pulse time of 10 μs. As the forcing frequency is increased, the pulse time remains constant meaning that the time when the plasma is off and the electrode is cooling becomes shorter. It was thought that the combination of the shorter cooling time and the anode being forced to carry twice the current of the cathode was leading to the electrode erosion. In order to alleviate this issue, it was decided to enlarge the anode holes in order to allow for installation of 1.5 mm electrodes. This would reduce the current density in the electrode and help to cool the electrode more quickly, hopefully allowing higher forcing frequencies to be tested. Based on the trend shown in Figure 18, it was theorized that the higher forcing frequencies would yield larger reductions in tonal amplitude.

Figure 19: Erosion Effects on Electrodes

4.3. – Initial Testing: 1.5 mm Anodes

In order to accommodate the larger anodes, the existing holes in the plasma extension were enlarged using a hand drill and increasing bit sizes. The electrodes were successfully painted and installed and were found to be capable of sustaining forcing frequencies up to 40 kHz before being eroded. Additionally, run times were greatly increased over the previous configuration and were not a major factor for the rest of the experiment. Forcing frequencies tested with the 1.5 mm anodes were 1 to 10 kHz in 1 kHz intervals, 10 to 20 kHz in 2 kHz intervals, and 20 to 40 kHz in 5 kHz intervals. The SPL spectrum for the 8 kHz frequency is overlayed with the baseline case as shown in Figure 20. This shows similar results with the previous configuration as the amplitude of the tone produced by the plasma actuators was still 150 dB. The effect on the cavity tone remained similar as well. In fact the 1.5 mm configuration exhibits a slightly smaller reduction in the tonal amplitude than was seen with the 1 mm anode. Figure 21 shows the change in tonal amplitude for each forcing frequency tested with the 1.5 mm anode. Interestingly, there was an increase in tonal amplitude at lower forcing frequencies and the 1.5 mm anode configuration was less effective at tone suppression than with the 1 mm configuration for all forcing frequencies tested. This is demonstrated in Figure 22 which compares the change in the amplitude of the 3 kHz tone for both anode sizes. It should be noted that the data in Figure 22 is from sensor 7 only but this is representative of all measurements taken. Thus the improvements in operation gained with larger anodes seem to come at a trade-off to actuator effectiveness.

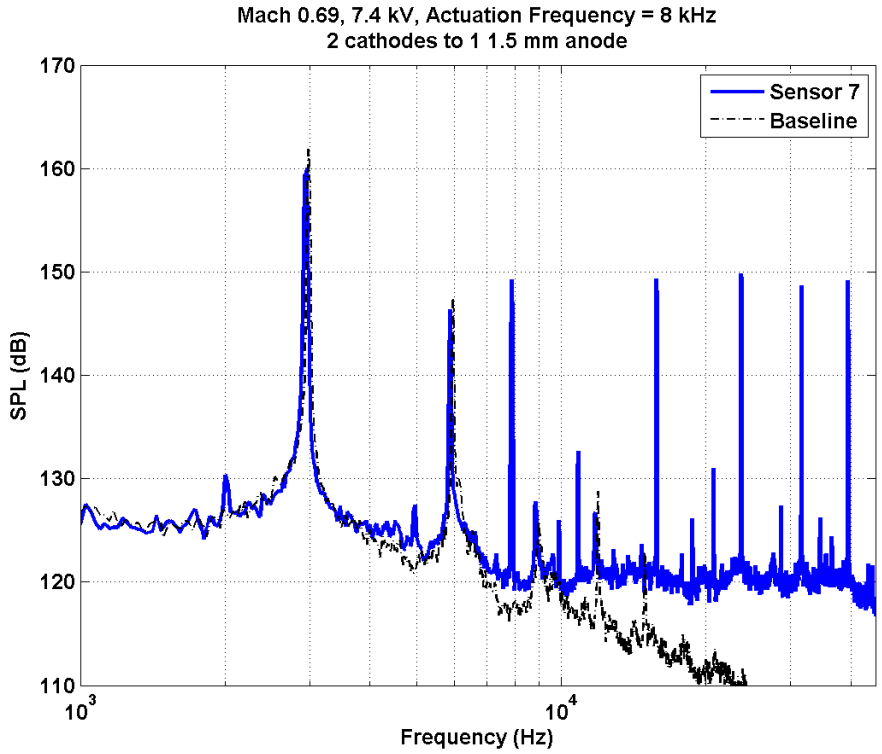

Figure 20: Mach 0.69 - 8 kHz forcing - 1.5 mm anode

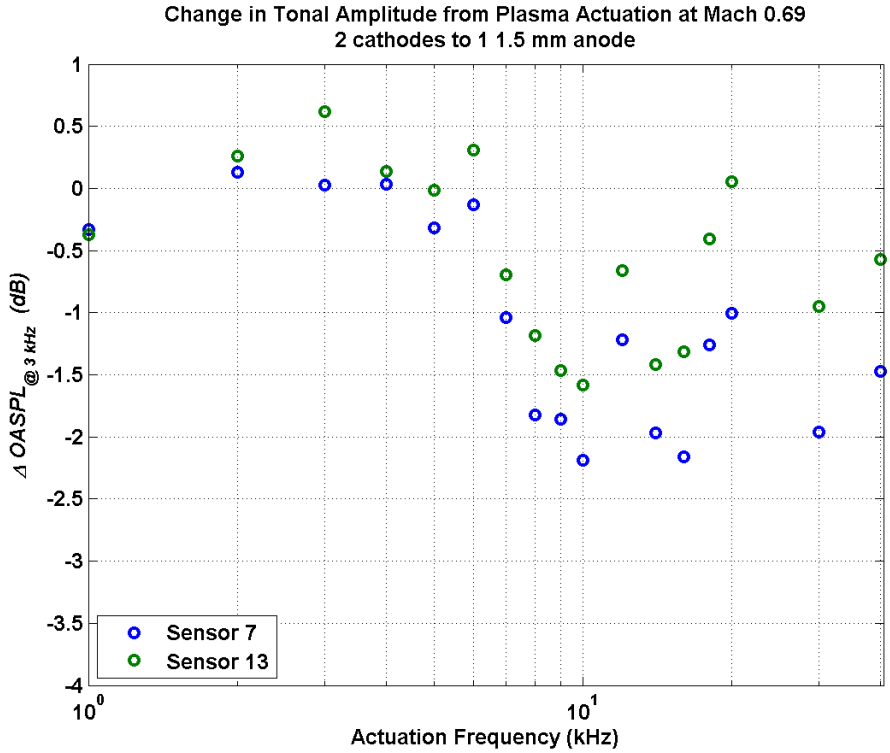

Figure 21: Change in Tonal Amplitude with 1.5 mm Anode

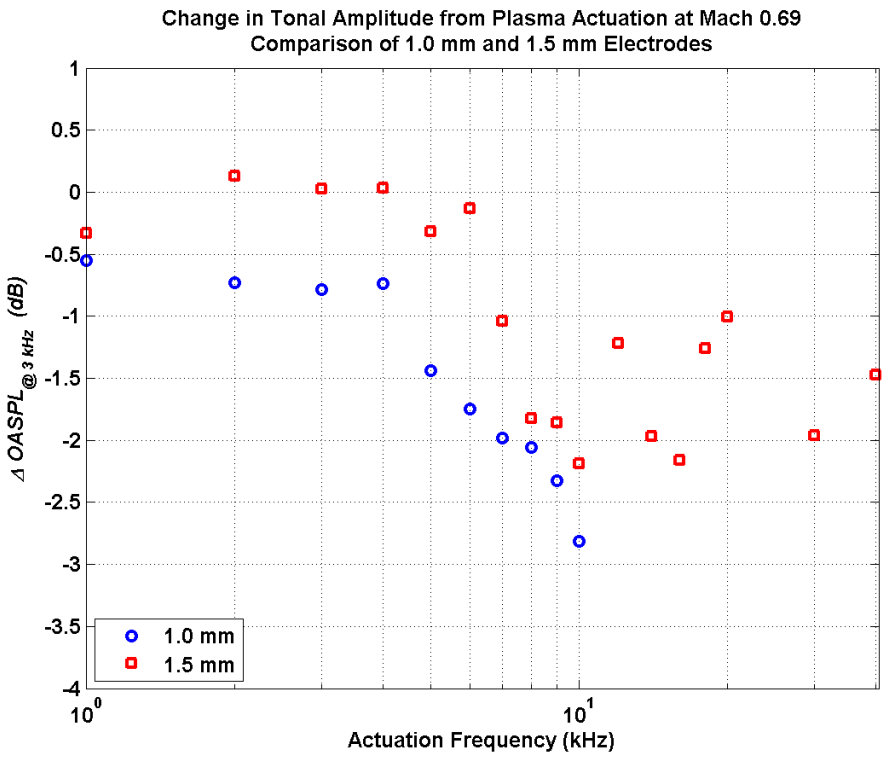

Figure 22: Comparison of Changes in Tonal Amplitude vs. Forcing Frequency and Anode Size

While the change to 1.5 mm anodes only reduced the anode to cathode separation by 0.25 mm, this reduces the resistance of the air separating the electrodes which reduced the breakdown voltage required to form plasma. This may be the cause of the reduced effectiveness exhibited by the larger anode configuration. The effect of reduced anode to cathode spacing is not completely understood so this trend may also be the result of another change made between the two sets of experiments. Regardless of cause, a difference in arc strength was observed with the larger anodes. Stronger arcs as seen in the original configuration appeared as a dark blue while weaker arcs as seen with the larger anodes were a lighter blue.

The larger anode configuration also showed a plateau in the tonal amplitude reduction at forcing frequencies greater than 10 kHz. Additionally, greater measurement

variability is seen between adjacent forcing frequencies in this region making the effect of higher forcing frequencies harder to quantify. Despite this difficulty, the marginal benefits of increased forcing frequency clearly decrease above 10 kHz. Additional measurement variability is exhibited between sensor 7 and sensor 13. This is shown in the baseline spectra of Figure 16 where sensor 7 generally shows a lower amplitude of pressure fluctuations. This may be anticipated due to the growth of the large scale structures in the shear layer as it travels downstream. In addition to this, sensor 7 shows a greater reduction in tonal amplitude at all frequencies as shown in both Figure 18 and Figure 21. Furthermore, both Figure 18 and Figure 21 show an increase in the variability of the sensor measurements with increasing forcing frequency. This is indicated by a increasing separation between the sensor 7 and sensor 13 data points as forcing frequency is increased. While not conclusive, this may be due to the differences in sensor position making one senor more susceptible to the influence of cavity acoustics than the other sensor.

Despite some interesting trends gathered from these experiments, none of the data exhibited suppression of the cavity tone by more than 3 dB. Thus these results did not satisfy the original goal of effective suppression of cavity tones. Once it had been verified that the current configuration was not as effective at tone suppression as had been hoped, work began on designing a new plasma actuator extension in order to achieve better results.

4.4. – Plasma Extension Redesign

The primary goals of redesigning the extension were to improve the effectiveness of the plasma actuators at controlling the cavity flow and to improve the operability of the actuators by producing stronger arcs and allowing longer running times without having to repaint the electrodes. Based on these considerations and prior research efforts conducted at the GDTL (Utkin et al., 2007), it was decided to revert to the original LAFPA configuration of one cathode and one anode per actuator. A Matlab script was then used to generate designs for varying anode to cathode spacings. To prevent unintended arcing, the spacing between adjacent actuators was kept larger than the spacing between the anode and cathode of an actuator. Similar precautions were taken to avoid unintended arcing to the wall of the facility. After generating several different possible designs, two designs with differing anode to cathode spacing were selected to be produced. Table 1 shows the primary design parameters for each of these redesigns compared to the original configuration. Only Redesign #1 was received in time for it to be tested and included in this research.

Table 1: Plasma Actuator Extension Redesign Parameters

	No. of Actuators	**Anode - Cathode Spacing (mm)**	**Actuator Spacing (mm)**	**Actuator - Wall Spacing (mm)**	**Coverage (%)**
Original	5	4.00	5.00	8.00	53%
Redesign #1	8	3.50	5.20	5.90	37%
Redesign #2	10	3.00	4.00	5.10	39%

4.5. – Redesigned Extension Testing

After verifying that the Mach 0.69 flow over the cavity remained unchanged with the new actuator extension in place, two sets of experiments were conducted. The first experiment was exactly similar to the previous experiments with forcing frequencies of the form X kHz – X % duty cycle tested to maintain a constant plasma pulse of 10 μs. The second set of experiments used forcing frequencies with 20% duty cycle to examine the effect of changing duty cycle on the plasma actuators' authority. Forcing frequencies from 1 to 40 kHz were tested in both experiments. Figure 23 shows the SPL obtained for forcing at 8 kHz with 10 μs plasma pulses and Figure 24 shows the SPL with 8 kHz forcing and 20% duty cycle. Both SPL's are representative of all data obtained in this experiment. Figure 25 shows the change in amplitude of the 3 kHz tone for all forcing frequencies tested with the 10 μs plasma pulse. Figure 26 is a similar figure for the 20% duty cycle forcing frequencies tested.

The primary results of this test are shown in Figure 25 and Figure 26 where it can be seen that the redesigned configuration is not a significant improvement over the original design as the maximum tone suppression is less than 2 dB. The SPL's shown in Figure 23 and Figure 24 show that there is a possible effect of duty cycle however, as the high frequency noise is reduced with the 20% duty cycle compared to the 10 μs pulse. This effect was observed at all forcing frequencies below 20 kHz (where these two duty cycles produce the same forcing function). This reduction in high frequency noise may be due to the fact that the induced pressure fluctuations from the actuator are slightly weaker for the 20% duty cycle case or may be due to EMI. Thus further research in the form of current and voltage measurements are needed to verify this.

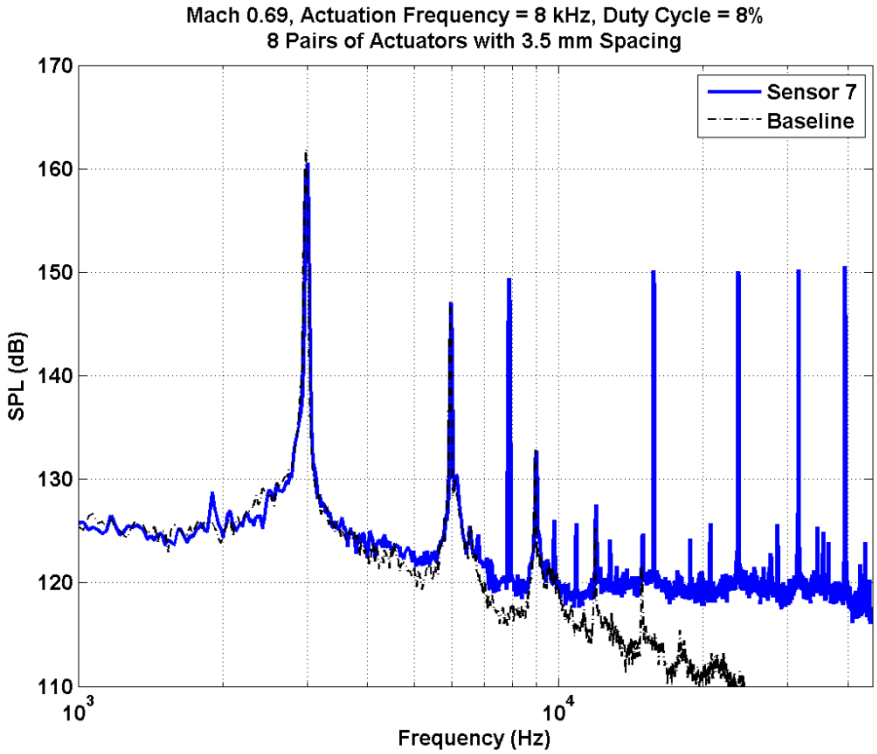

Figure 23: Mach 0.69 - 8 kHz – 8% duty cycle forcing - 1.0 mm anode

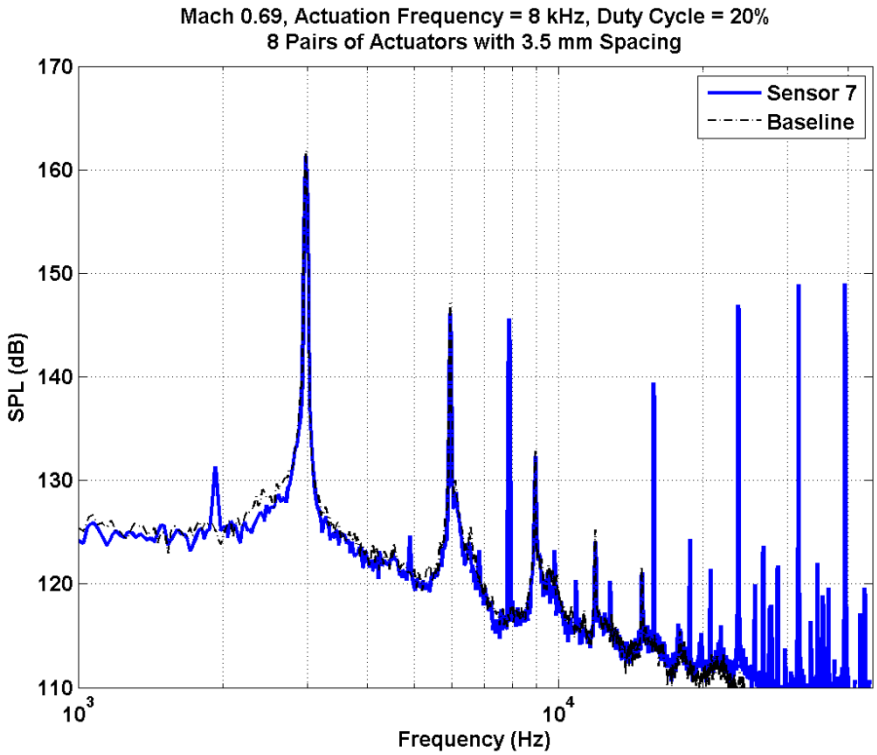

Figure 24: Mach 0.69 - 8 kHz – 20% duty cycle forcing - 1.0 mm anode

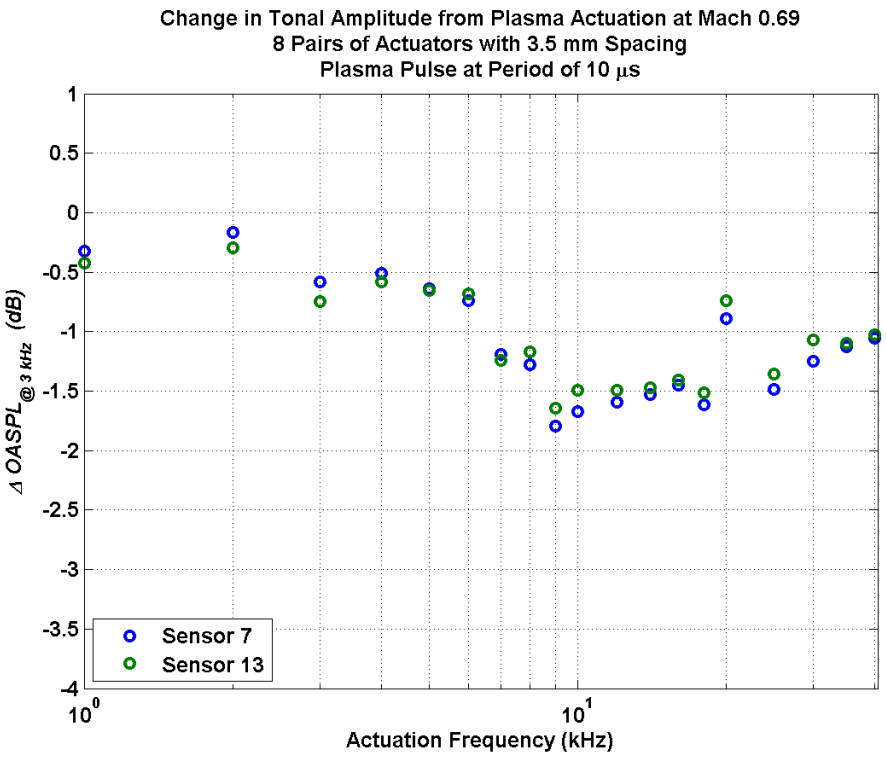

Figure 25: Change in Tonal Amplitude with 1.0 mm Anodes and 10 μs Plasma Pulse

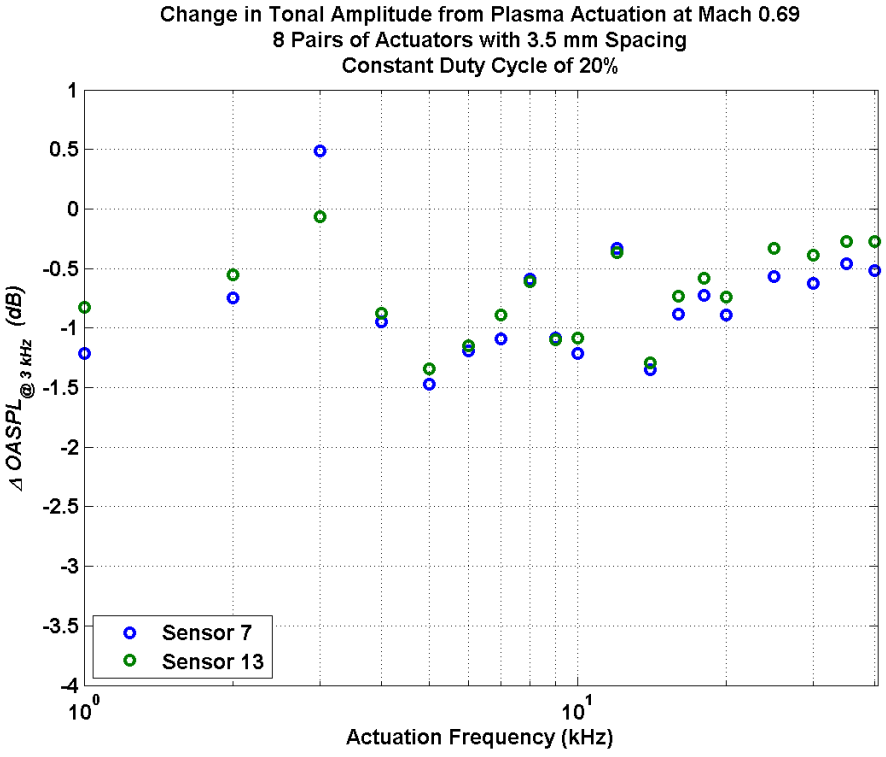

Figure 26: Change in Tonal Amplitude with 1.0 mm Anodes and 20% Duty Cycle

4.6. – Low Mach Number Experimentation

The final set of experiments performed in this research involved attempting to control a cavity flow with lower power using the redesigned extension. The Mach 0.34 baseline case used can be seen in Figure 27 and contains a resonant tone at 3.8 kHz with an amplitude of approximately 143 dB. The amplitude of the fluctuating pressure of the tone is thus approximately one order of magnitude (20 dB) lower than the tone for the Mach 0.69 baseline. For this experiment forcing frequencies from 1 to 10 kHz were tested. Additionally, plasma pulses of 10, 20, and 40 μs were tested for each frequency.

Forcing at 6 kHz proved to be the most effective at tone suppression and the SPL's obtained for this case can be seen below. Figure 28, Figure 29, and Figure 30 show the results for 6 kHz forcing using plasma pulses of 10, 20, and 40 μs, respectively where the effect of duty cycle can be seen in both amount of tone suppression and the high frequency noise level. Similar to the results of Figure 23 and Figure 24 above, increased duty cycle is seen to result in decreased high frequency noise. More importantly, increasing the plasma pulse from 10 μs to 20 μs resulted in significantly higher tone suppression (approximately 10 dB). Further increasing the pulse period to 40 μs produced slightly higher attenuation (approximately 12 dB), but the marginal benefits of increasing the plasma pulse time are much lower. Despite this, the plasma actuators performed significantly better at suppressing the resonant tone generated in the Mach 0.34 flow than the tone generated by the Mach 0.69 flow.

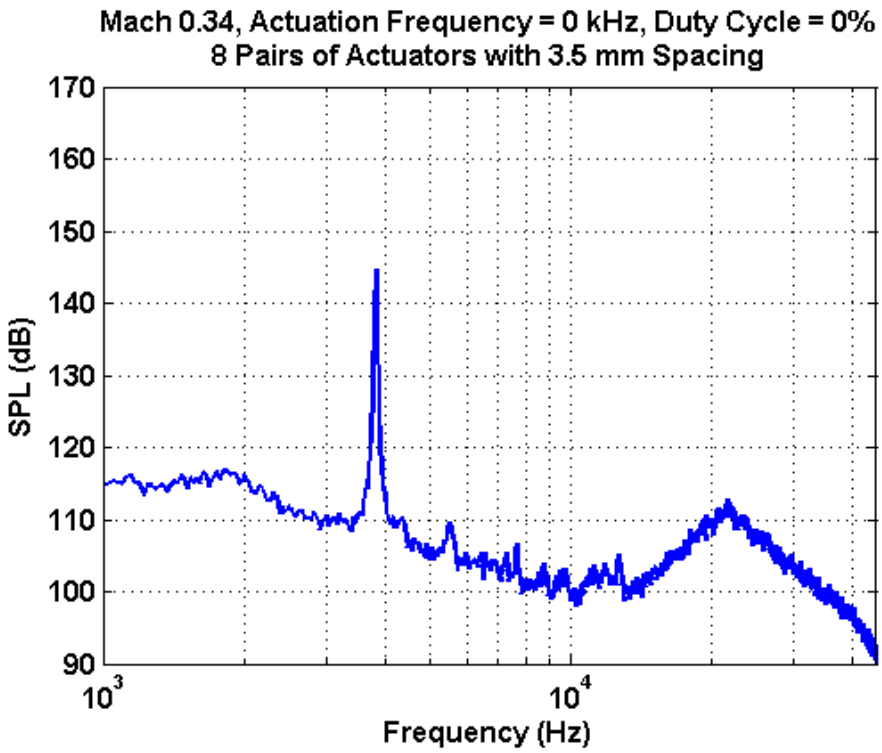

Figure 27: Mach 0.34 – Baseline

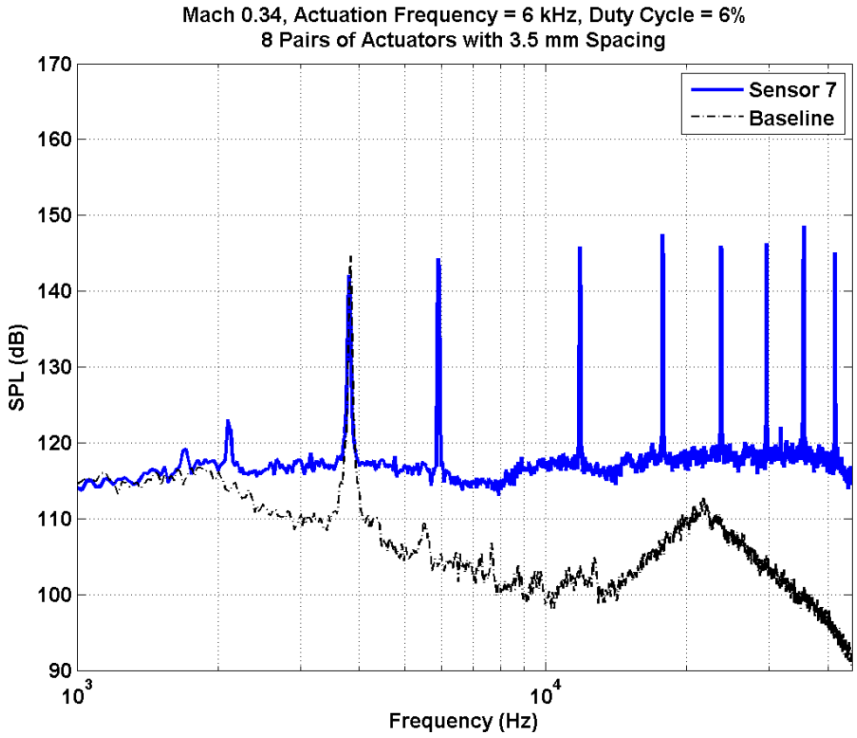

Figure 28: Mach 0.34 - 6 kHz – 6% duty cycle (10 µs pulse) - 1.0 mm anode

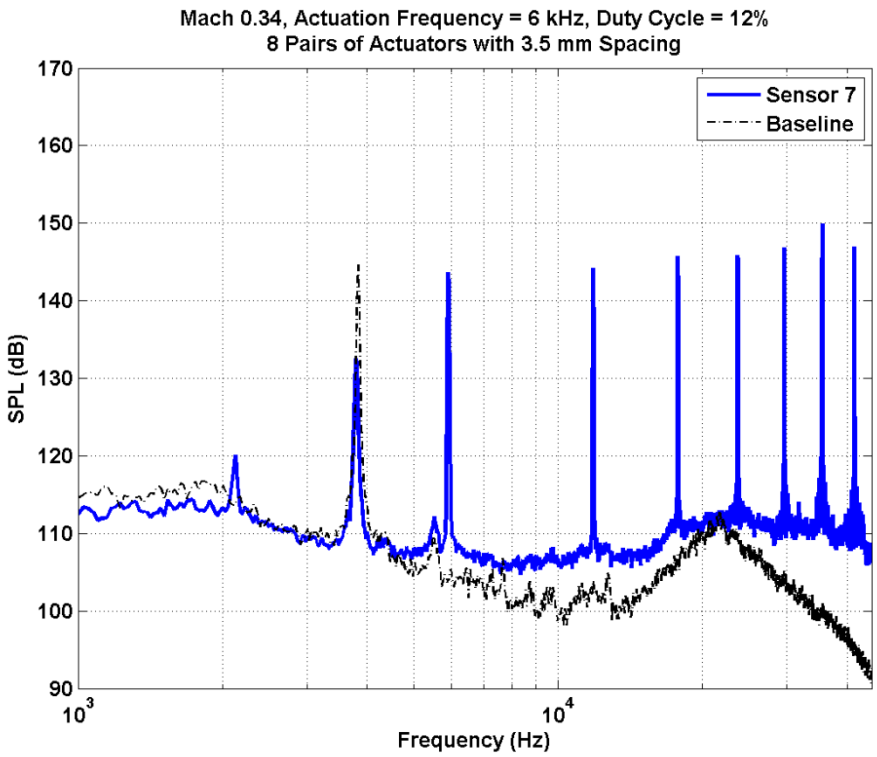

Figure 29: Mach 0.34 - 6 kHz – 12% duty cycle (20 µs pulse) - 1.0 mm anode

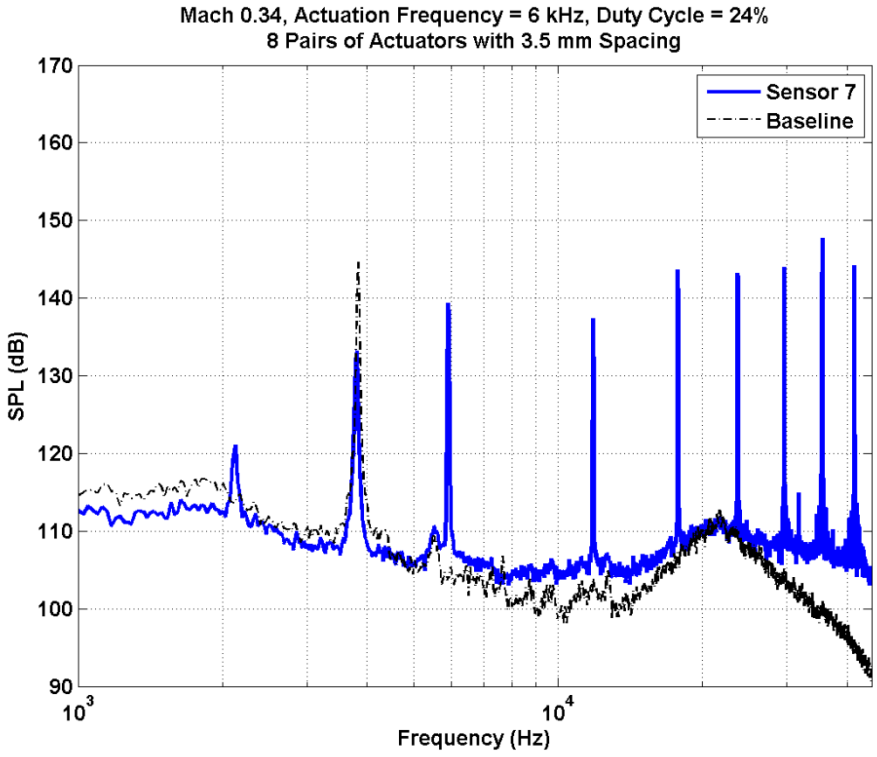

Figure 30: Mach 0.34 - 6 kHz – 24% duty cycle (40 µs pulse) - 1.0 mm anode

CHAPTER 5

CONCLUSIONS AND FUTURE WORK

Prior research has shown that a compression driver was capable of attenuating the tone generated by flow over a shallow cavity by up to 20 dB at Mach 0.30. The compression driver showed a loss of authority over the flow at Mach numbers higher than 0.40 due to insufficient bandwidth and amplitude of actuation. In an attempt to overcome this limitation, LAFPA's were installed along the leading edge of a shallow test cavity due to their ability to generate strong pressure fluctuations that could be used to influence the shear layer. The cavity tested was 1.00" in length, 0.25" deep, and 3.00" across.

The cavity flow was characterized by performing a Mach sweep from Mach 0.55 to Mach 0.80 and pressure measurements were obtained using Kulites connected to a data acquisition system running LabVIEW. A baseline resonating flow was selected at Mach 0.69 with a 3 kHz tone of approximately 160 dB amplitude.

The plasma actuator extension was manufactured from boron nitride machinable ceramic and fitted with 5 plasma actuators. Each actuator contained two cathodes which shared a common anode with a spacing of 4.00 mm. The spacing between adjacent actuators was 5.00 mm. Originally all actuators were 1.00 mm in diameter but due to operability problems caused by electrode erosion, the cathode size was modified to a diameter of 1.50 mm. Using forcing frequencies from 1 to 40 kHz

with a constant 10 μs plasma pulse, neither configuration showed significant attenuation of the resonant tone, so two new extensions were designed.

Due to the operability problems associated with the common anode configuration, the new actuator extensions were designed using the typical LAFPA design of one cathode and one anode per actuator. Only one redesigned extension was received in time to be tested for this research however. Despite the testing of forcing frequencies with constant plasma pulse of 10 μs and constant 20% duty cycle, the redesigned extension produced only small attenuation of the resonant tone.

Due to the lack of actuator effectiveness at Mach 0.69, it was decided to test a lower power flow at Mach 0.34. For this case the resonant tone at 3.8 kHz of approximately 140 dB amplitude was able to be suppressed by up to 12 dB with actuation at 6 kHz. Additionally the high frequency noise tended to be reduced with increased duty cycle.

Since the redesigned extension was only available to be tested for a short time however, these results need verification. Firstly, both the attenuation shown and the effects of increased duty cycle need to be examined to ensure that no EMI effects are present. Furthermore more duty cycles need to be tested to verify the trends observed for the Mach 0.34 flow. Lastly, the second redesigned extension needs to be tested and the results compared to those of the other two extensions.

Despite the ineffectiveness of the plasma actuators at suppressing cavity tones for higher Mach numbers, several important accomplishments were achieved in this research. Firstly, plasma actuators were successfully installed and tested in the cavity facility. The actuators were shown to function reliably and correctly even with very close actuator

spacing along the cavity leading edge. Furthermore, Kulite pressure data was successfully taken in close proximity to the large sources of EMI presented by the actuators.

From a flow control perspective, two main conclusions can be reached. Firstly, it appears that plasma actuator duty cycle play a much larger role in effective actuation than was originally thought. Even for the Mach 0.34 flow, a 20 μs plasma pulse was required for successful tone suppression which is in contrast to optimum pulse periods with other LAFPA applications. Furthermore duty cycle appears to have an effect on high frequency noise for the cavity flow, although this has yet to be conclusively verified. Lastly, the 12 dB tonal suppression observed for the Mach 0.34 flow demonstrates promise for successful tone suppression at higher Mach numbers. The results suggest that actuator effectiveness is determined by the relative amplitudes of the resonant tone and the actuator induced pressure fluctuations. For the high Mach number case, the actuators produced a tone that was approximately 10 dB lower than the resonant tone and were ineffective. In contrast, the Mach 0.34 flow has a resonant tone with amplitude that is approximately the same order of magnitude as the pressure fluctuations induced by the actuators. Since the actuators showed much greater authority over the Mach 0.34 flow, this suggests that similar results may be obtained if the actuators can be made to induce stronger pressure fluctuations at the shear layer. Since the original goal of this research was the suppression of a cavity tone generated by a high Mach number flow, much of the future work will be focused on design modifications to allow the effectiveness shown to be translated to high velocity flows.

REFERENCES

Bjorge, S., Reeder, M., Subramanian, C., Crafton, J., Fonov, S., "Flow Around an Object Projected from a Cavity into a Supersonic Freestream," *AIAA Journal* 43.7 (2005): 1465-1475.

Cattafesta, L., Garg, S., Choudhari, M., Li, F., "Active Control of Flow-Induced Cavity Resonance," 1997, AIAA Paper 1997-1804.

Cattafesta, L., Garg, S., Shukla, D., "Development of Piezoelectric Actuators for Active Flow Control," *AIAA Journal* 39.8 (2001), pp. 1562-1568.

Cattafesta, L., Kegerise, M., Jones, G., "Experiments on Compressible Flow-Induced Cavity Oscillations," AIAA Paper 98-2912, 1998.

Cattafesta, L., Williams, D., Rowley, C., Alvi, F., "Review of Active Control of Flow-Induced Cavity Resonance," AIAA Paper 2003-3567, 2003.

Debiasi, M., and Samimy, M., "Logic-Based Active Control of Subsonic Cavity Flow Resonance," *AIAA Journal* 42.9 (2004): pp. 1901-1909.

Halliday, D., Resnick, R., Walker, J., *Fundamentals of Physics: Extended. 6th Ed.*, New York: John Wiley & Sons, Inc., 2001.

Little, J., "Development and Application of a Visualization Technique for Baseline and Controlled Cavity Flow," Undergraduate Thesis, 2004.

Little, J., Debiasi, M., Samimy, M., "Flow Structure and Baseline Subsonic Cavity Flows," AIAA Paper 2006-480, 2006.

McGregor, O. W. and White, R. A., "Drag of Rectangular Cavities in Supersonic and Transonic Flow Including the Effects of Cavity Resonance," *AIAA Journal* 8.11 (1970): pp. 1959-1964.

Mitchell, D., "Control of High Speed Cavity Flow using Plasma Actuators," Undergraduate Thesis, 2006.

Pope, Stephen B., *Turbulent Flows*, New York: Cambridge University Press, 2000.

Rockwell, D., and Naudascher, E., "Review – Self Sustaining Oscillations of Flow past Cavities," *Journal of Fluids Engineering*, Vol. 100, 1978, pp. 152-165.

Samimy, M., Adamovich, I., Webb, B., Kastner, J., Hileman, J., Keshav, S., and Palm, P., "Development and Characterization of Plasma Actuators for High Speed and Reynolds Number Jet Control," *Experiments in Fluids*, Vol. 37, No. 4, pp. 577-588, 2004.

Samimy, M., Kim, J.-H., Kastner, J., Adamovich, I., and Utkin, Y., "Active Control of High Speed and High Reynolds Number Jets Using Plasma Actuators," *Journal of Fluid Mechanics*, Vol. 578, pp. 305-330, May 2007.

Utkin, Y., Keshav, S., Kim, J.-H., Kastner, J., Adamovich, I., and Samimy, M., "Use of Localized Arc Filament Plasma Actuators for High Speed Jet Control," *Journal of Physics D: Applied Physics*, Vol. 40, pp. 685-694, February 2007.

Williams, D. R., Fabris, D. and Morrow, J., "Experiments on Controlling Mulitiple Acoustic Modes in Cavities," AIAA Paper 2000-1903, 2000.

Williams, D.R., Rowley, C., Colonius, T., Murray, R., MacMartin, D., Fabris, D., and Albertson, J., "Model-Based Control of Cavity Oscillations – Part I: Experiments," AIAA Paper 2002-0971, 2002.

APPENDIX A

Plasma Actuator Extension Drawings

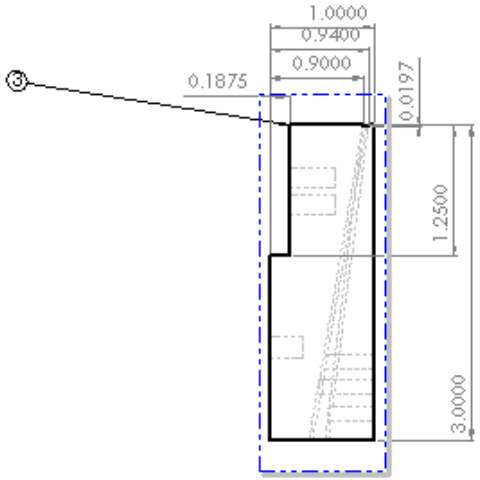

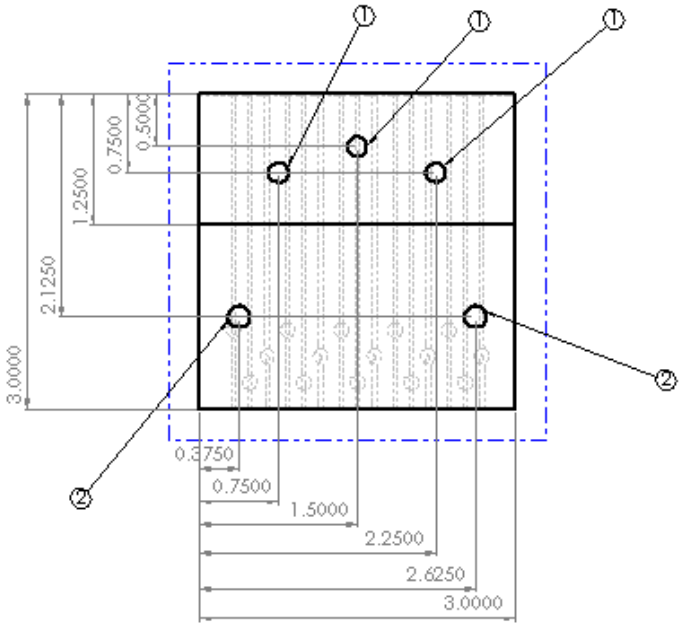

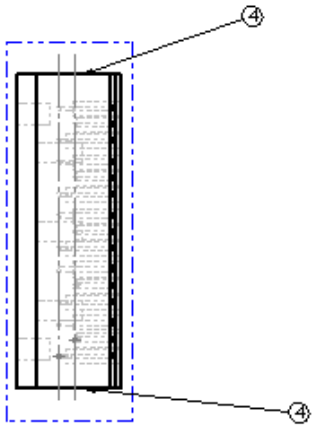

Item No.	Quantity	Hole Description
1	3	#10-24 UNC threaded Holes for Plastic Philips Head Bolts 0.4375" deep
2	2	#10-24 UNC threaded Holes for Plastic Philips Head Bolts 0.3125" deep
3		Must be even and aligned with callout 3 on 1 - Actuator_Spacer piece
4		Boron piece cannot be wider than 1 - Actuator_Spacer piece

Tolerance is +/- 0.005
Do Not round corners. All corners left straight.

Material: Boron Nitride AX05 Plate

Simultan. Pressure & PIV Actuator Assembly

Part Name: 1 - Actuator_Boron View 1

Gas Dynamics and Turbulence Laboratory
The Ohio State University

Doug Mitchell 08-15-2006

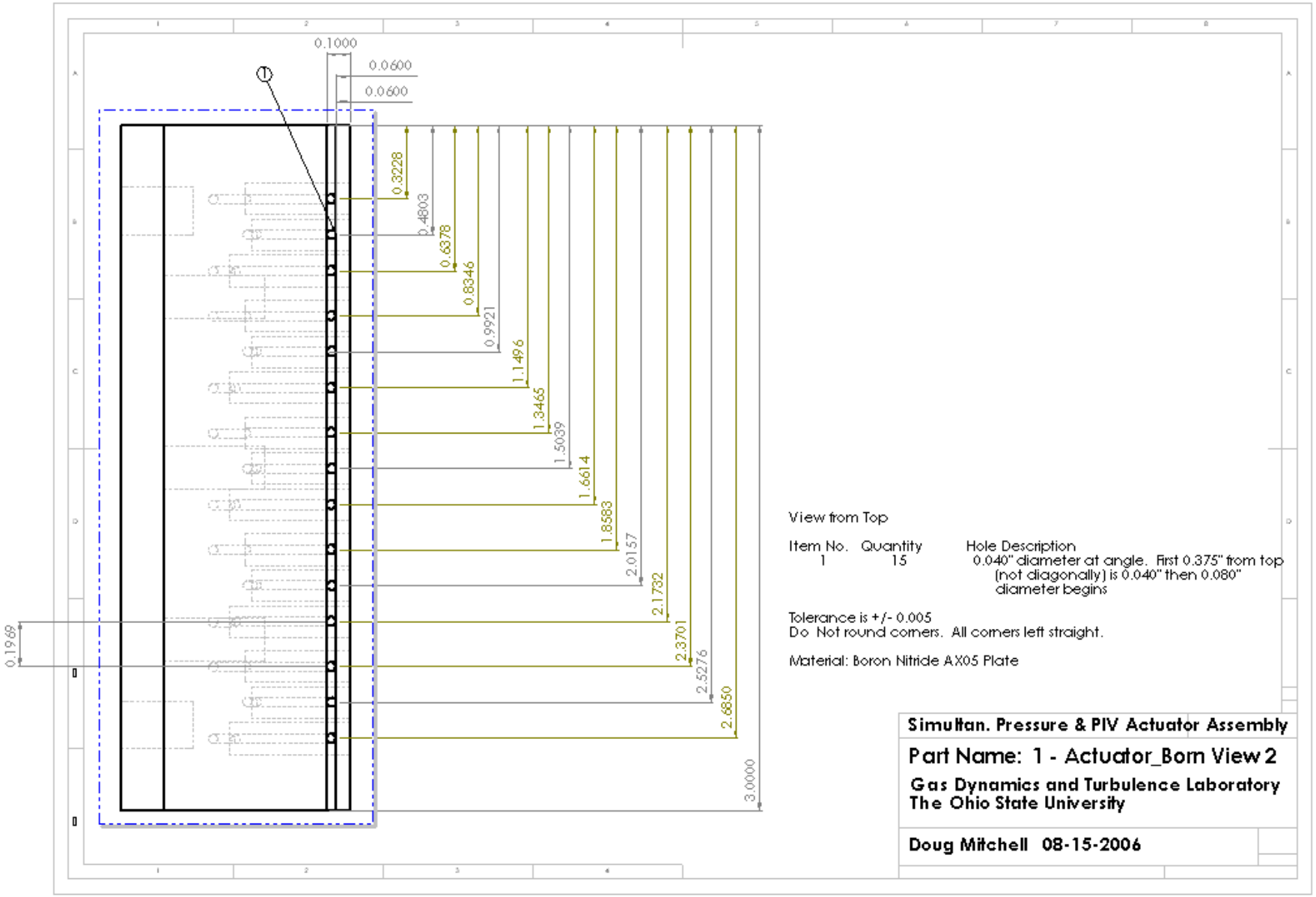
0.1000
0.0600
0.0600
0.3228
0.4803
0.6378
0.8346
0.9921
1.1496
1.3465
1.5039
1.6614
1.8583
2.0157
2.1732
2.3701
2.5276
2.6850
3.0000
0.1969
View from Top
Item No. Quantity
1 15
Hole Description
0.040" diameter at angle. First 0.375" from top (not diagonally) is 0.040" then 0.080" diameter begins
Tolerance is +/- 0.005
Do Not round corners. All corners left straight.
Material: Boron Nitride AX05 Plate
Simultan. Pressure & PIV Actuator Assembly
Part Name: 1 - Actuator_Born View 2
Gas Dynamics and Turbulence Laboratory
The Ohio State University
Doug Mitchell 08-15-2006

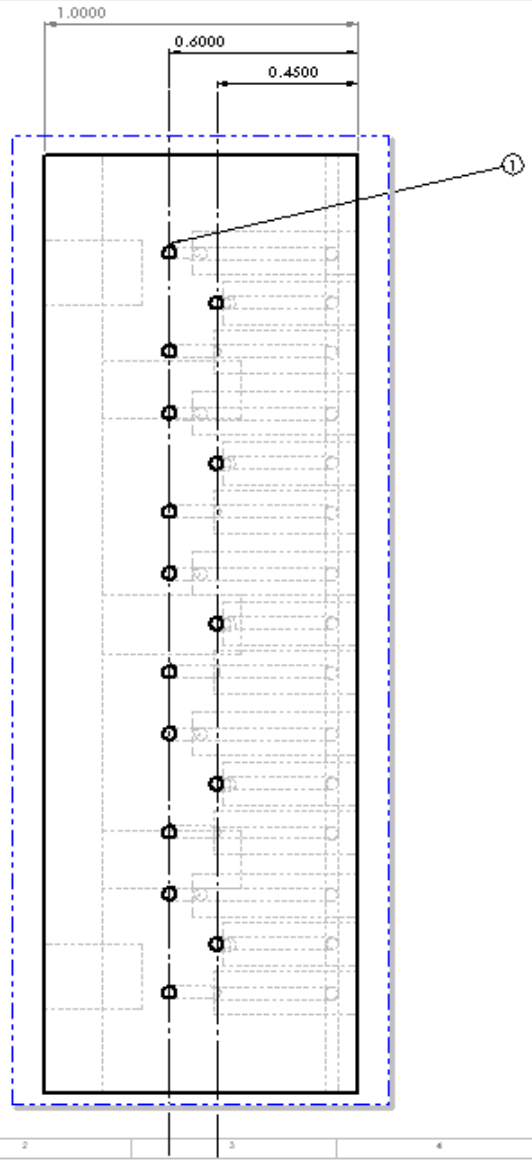

View from Bottom

Item No.	Quantity	Hole Description
1	15	0.080" diameter at angle. First 0.375" from top (not diagonally) is 0.040" then 0.080" diameter begins

Tolerance is +/- 0.005
Do Not round corners. All corners left straight.

Material: Boron Nitride AX05 Plate

Simultan. Pressure & PIV Actuator Assembly

Part Name: 1 - Actuator_Boron View 3

Gas Dynamics and Turbulence Laboratory
The Ohio State University

Doug Mitchell 08-15-2006

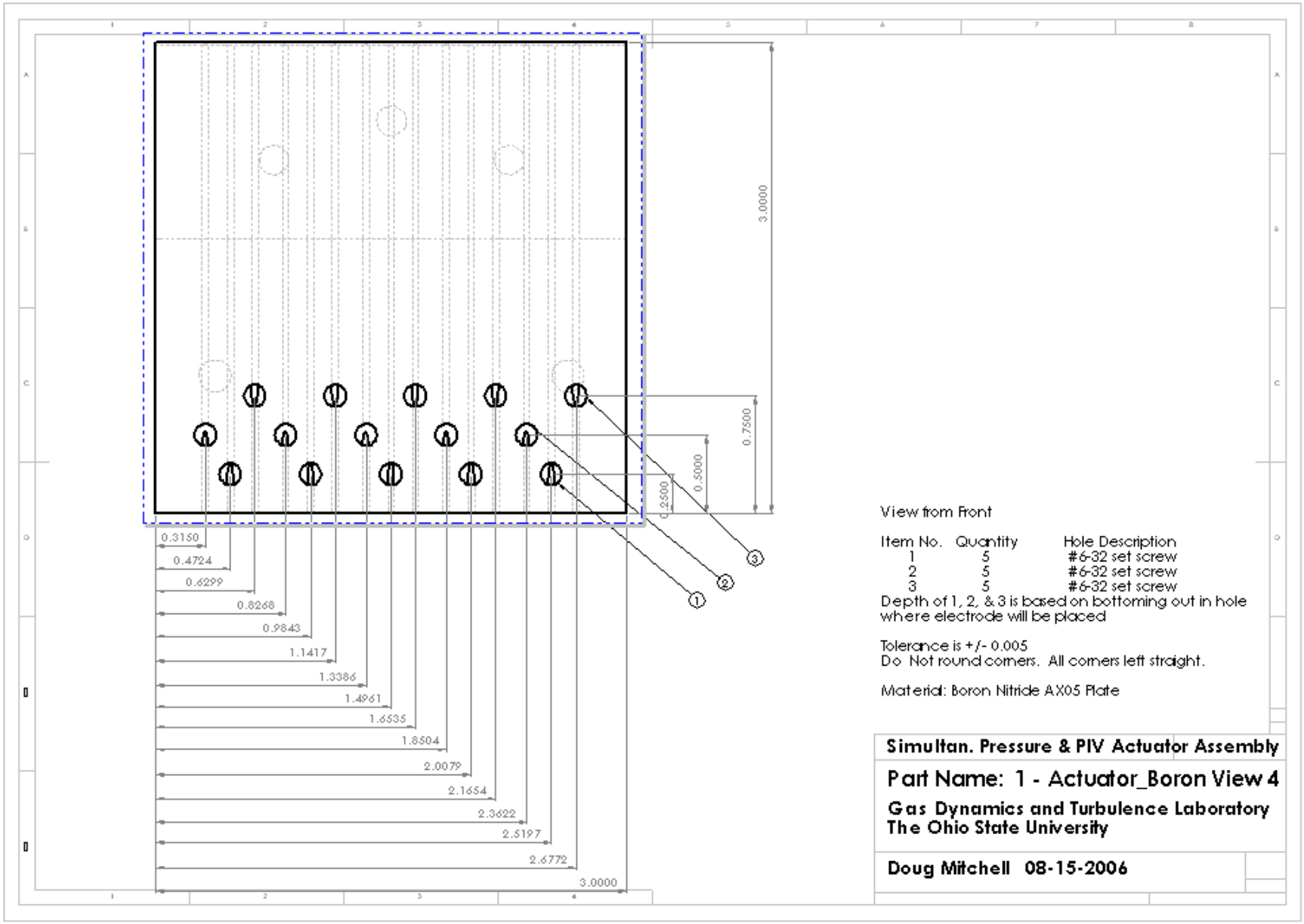

View from Front

Item No.	Quantity	Hole Description
1	5	#6-32 set screw
2	5	#6-32 set screw
3	5	#6-32 set screw

Depth of 1, 2, & 3 is based on bottoming out in hole where electrode will be placed

Tolerance is +/- 0.005
Do Not round corners. All corners left straight.

Material: Boron Nitride AX05 Plate

Simultan. Pressure & PIV Actuator Assembly

Part Name: 1 - Actuator_Boron View 4

Gas Dynamics and Turbulence Laboratory
The Ohio State University

Doug Mitchell 08-15-2006

APPENDIX B

Wiring Schematics

Original Wiring Design

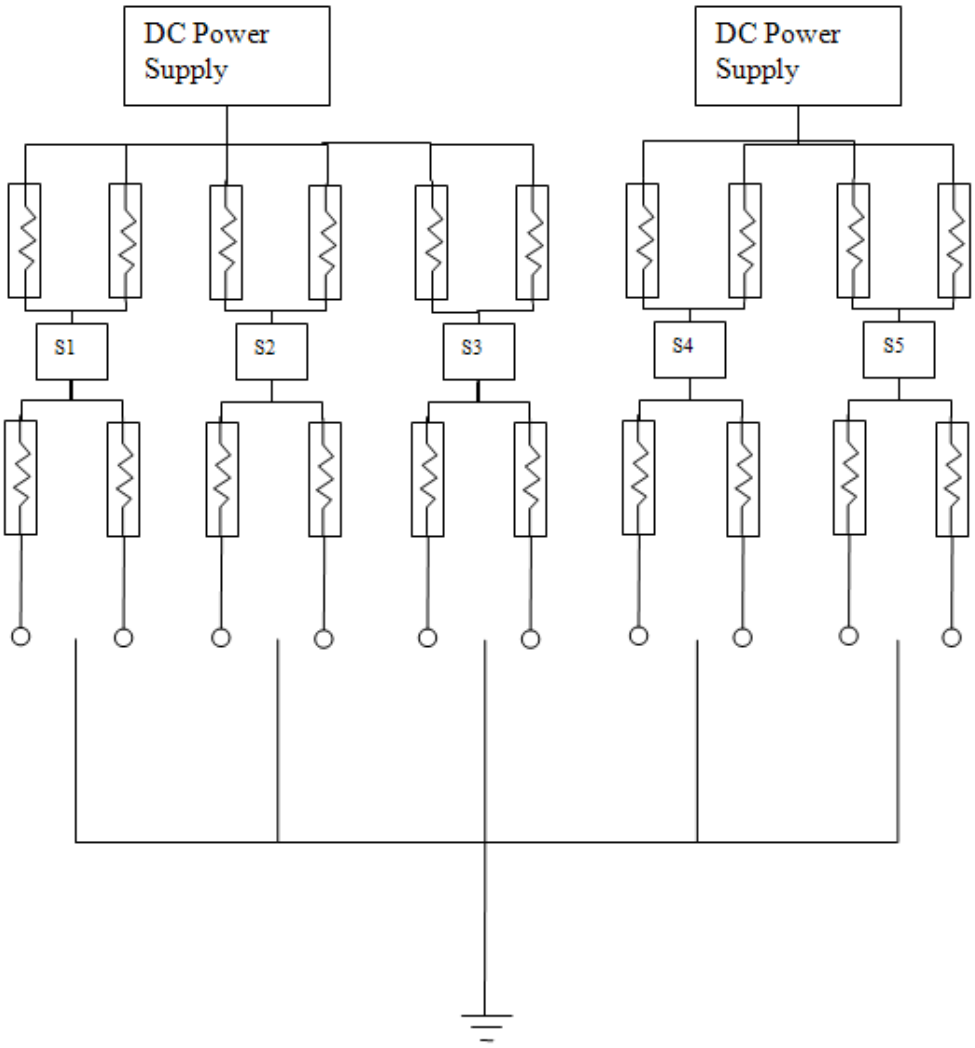

Final Wiring Design